The Dissertation Committee for Enrica Quartini
certifies that this is the approved version of the following dissertation:

## The distribution of geothermal flux in West Antarctica

Committee:

_____
Donald D. Blankenship, Supervisor

_____
Duncan A. Young, Co-Supervisor

_____
Ian W. D. Dalziel

_____
Luc Lavier

_____
Dustin M. Schroeder

_____
Clark R. Wilson

# The distribution of geothermal flux in West Antarctica

## by

## Enrica Quartini

**DISSERTATION**

Presented to the Faculty of the Graduate School of

The University of Texas at Austin

in Partial Fulfillment

of the Requirements

for the Degree of

**DOCTOR OF PHILOSOPHY**

THE UNIVERSITY OF TEXAS AT AUSTIN

December 2018

# Acknowledgments

# The distribution of geothermal flux in West Antarctica

Enrica Quartini, Ph.D.
The University of Texas at Austin, 2018

Supervisors:   Donald D. Blankenship
Duncan A. Young

The West Antarctic Ice Sheet (WAIS) contains the equivalent of $\sim 3.3$ m of global sea level rise and is the largest ice sheet on Earth grounded almost entirely below sea level. This is a potentially unstable configuration that makes WAIS prone to rapid collapse during interglacial periods, a condition known as marine instability. One poorly understood but possibly dominant process in past and future collapses of WAIS is its coupling with the underlying West Antarctic Rift System (WARS), a Jurassic through Cenozoic region of intracontinental extension characterized by active volcanism. WARS' topographic range, complex tectonic history, and volcanism exert a large influence on the distribution of elevated geothermal flux, a critical but poorly constrained ice sheet boundary condition for the collapse-prone marine-based WAIS. Examples of elevated geothermal flux have been observed throughout the West Antarctic Rift System (WARS). Uncertainties remain however on the timing, evolution, and extent of both the WARS and its volcanism.

In this dissertation I analyze magnetic anomalies in the context of other aerogeophysical data in central West Antarctic Rift System (WARS) in order to

evaluate the distribution of potential hotspots in the region. I identify three different regions with distinct magnetic character and correlate each region to specific stages of tectonic and magmatic activity in WARS. My interpretation supports both the hypothesis that Marie Byrd Land was tectonically and magmatically reactivated multiple times during the Jurassic and Cenozoic and that a hotspot was emplaced there later in the Cenozoic.

I also use the approach described by Schroeder et al. (2014a) to investigate the distribution of elevated and possibly transient geothermal flux along Marie Byrd Land and the Siple Coast of West Antarctica. I employ a vast archive of radar sounding datasets in West Antarctica and use coherent phase sensitive radar to constrain the geometry of subglacial water systems (Schroeder et al., 2013). Under constrained conditions, the amplitude of radar returns can be used with a subglacial water routing model to infer basal melt (Schroeder et al., 2014a). This technique is based on the assumption that the brightness of radar reflectors is proportional to the areal coverage by water at the ice-bed interface. The assumption is valid in the case of subglacial distributed canals, which have been proved to be the current subglacial water system dominating the Thwaites Glacier catchment in West Antarctica (Schroeder et al., 2013).

Once a ground water transportation system has been selected, the technique uses the bed topography and ice surface elevation to calculate the hydraulic head in a region, which gives information on the subglacial water flow direction and the extent of the upstream catchment. Both of these quantities are used to estimate the total water flow in the region. If the amount of water detected from the radar ampli-

tude analysis exceeds the estimates of total water flow, then an additional source of basal melting, such as geothermal flux, needs to be invoked. Comparing the results with previous assessments of water production due to basal friction (Joughin et al., 2009), the amount of water melt produced by geothermal flux can be estimated.

# Table of Contents

# List of Tables

# List of Figures

# Chapter 1

# Introduction

Bedrock plays an important role in ice sheet stability as it affects ice sheets' basal boundary conditions. The lithology, topography, and geological structure of the bed affect the thickness, surface slope, and flow of the overlying ice (Weertman, 1974; Blankenship et al., 2011b; Damiani et al., 2014). One critical yet poorly constrained boundary condition is geothermal flux, which can generate basal melt water and facilitate fast flow of interior ice towards the coast.

The West Antarctic Ice Sheet (WAIS) contains the equivalent of $\sim 3.3$ m of global sea level rise (Bamber et al., 2009) and is the largest ice sheet on Earth grounded almost entirely below sea level (Alley and Bindschadler, 2001; Johnson et al., 2008), an unstable condition known as marine instability which could cause run-away grounding line retreat(Weertman, 1974). It has been hypothesized that WAIS typically collapsed during interglacial periods (Scherer et al., 1998; Ackert et al., 2013; Bamber et al., 2009; Pollard and DeConto, 2009), and concerns have been raised that the marine instability will initiate in the coming century (Joughin et al., 2014; Pollard et al., 2015), sustaining rapid ice mass loss.

WAIS sits on the West Antarctic Rift System (WARS), a Jurassic to Cenozoic intracontinental extension zone of low topography that causes the central part

of the WAIS to reside 1-2 km below sea level. Moreover, WARS is characterized by elevated geothermal flux and active subglacial volcanism (Blankenship et al., 1993; Behrendt, 1999; Lough et al., 2013; Schroeder, 2014), which pose a potential threat to the collapse-prone WAIS.

Additionally, geothermal flux impacts the age structure of the deep ice sheet. The recently completed WAIS Divide ice core did not reach its age target due to an incomplete understanding of WARS basal geothermal flux. Constraining the distribution of geothermal flux would therefore help ice coring and rapid access efforts find high resolution records and sample the inception of the current WAIS.

## 1.1 Geothermal flux

Subglacial geothermal flux is a critical, yet poorly defined basal condition of the ice sheet. It affects both components of ice sheet flow: by producing melting at the base of the ice, it lubricates the base and allows sliding flow, and by altering the rheology of ice, which is sensitive to temperature, it enhances viscous flow of the ice column. While the impact of geothermal flux on ice flow is less significant in regions of fast flowing ice, such as along the coast, it is much more important in the cold and slowly moving ice of the interior.

Geothermal flux in the WARS region generates basal melt water and contributes to ice sheet instability by lubricating the base of the ice sheet and causing ice streams to speed up. Basal water allows sliding at the base of the ice in the area surrounding a heat anomaly and also sustains subglacial hydraulic systems which lubricate the ice sheet further downstream (Engelhardt et al., 1990; Kamb, 2001;
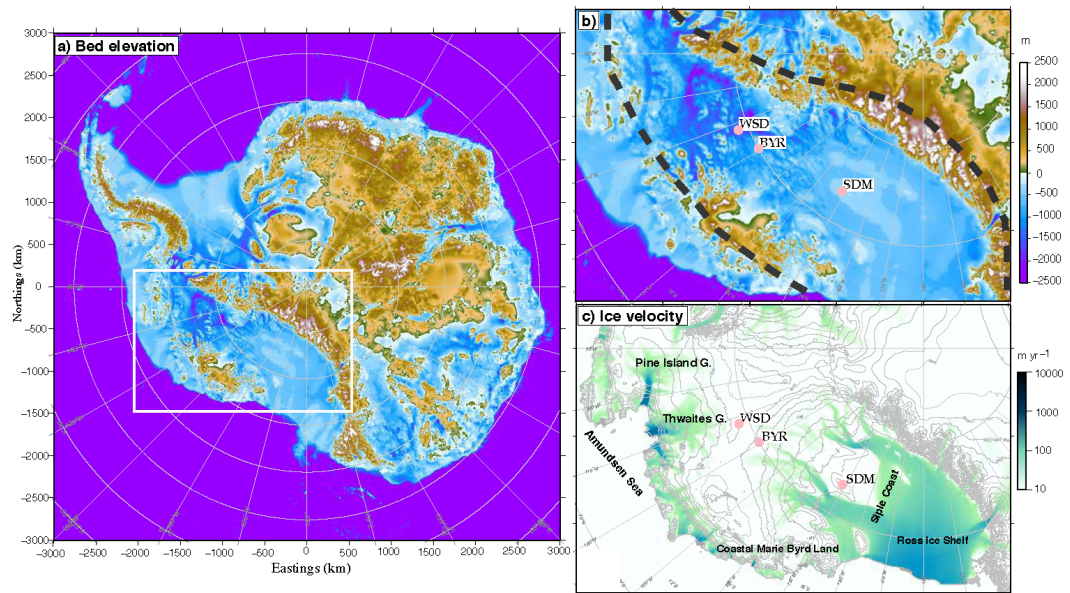
Figure 1.1: Study area. a) Antarctica bed elevation (Fretwell et al., 2013); EWM = Ellsworth-Whitmore Mountains, TAM = Transantarctic Mountains, MBL = Marie Byrd Land, SPC = Siple Coast, RSE = Ross Sea Embayment, AMS = Amundsen Sea Embayment; rectangle shows location of panels b) and c). b) Bed elevation in West Antarctica; thick dashed lines show hypothesized location of WARS rift flanks; pink dots locate ice core sites: WAIS divide (WSD), Byrd (BYR), and Siple Dome (SDM). c) InSAR ice surface velocity (Rignot et al., 2011a). Ice surface contours are shown in light gray (from Fretwell et al. (2013)); Pine Island Glacier and Thwaites Glaciers are indicated; dashed line shows the approximate location of WAIS ice divide.
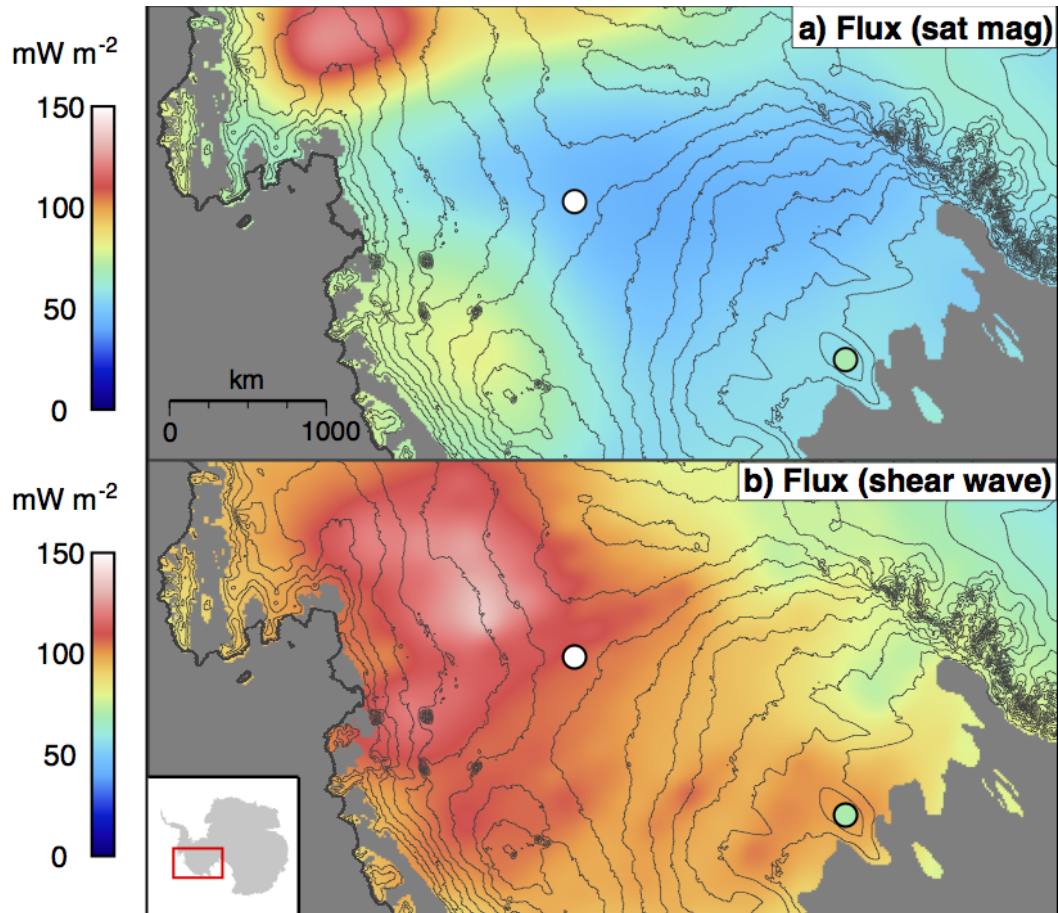
Figure 1.2: Estimates of West Antarctic heat flow. Two ice core based measurements of geothermal flux (WAIS Divide; Fudge et al. (2012) and Siple Dome; Engelhardt (2004b)) are indicated by circles, on same color scale. a) Satellite magnetics based geothermal flux (Fox Maule et al., 2005); b) Shear wave velocity estimated geothermal flux (Shapiro and Ritzwoller, 2004); Surface contours in gray from (Fretwell et al., 2013). Notably, most current ice sheet models use at least one of these widely discrepant models (e.g Christoffersen et al. (2014); Nowicki et al. (2013); Whitehouse et al. (2012))

4

Tulaczyk et al., 2000b; Tulaczyk et al., 2001). Therefore, the effects of geothermal flux on ice sheet dynamics are not confined to the localized area of elevated flux. Through a combination of channelized and distributed subglacial water systems, melt water produced in regions of high geothermal flux is transported to distal areas. In this way, geothermal flux has the potential to indirectly enhance ice flow in coastal regions as well, through the supply of melt water that further lubricates the bed and allows sliding.

The ice in the interior is much colder, higher in latitude and elevation, and slowly moving. There, geothermal flux represents the primary source of basal heat and therefore plays a large control on ice flow dynamics. Most importantly, the interior ice is much thicker and higher above flotation than the grounded-below-sea-level coastal ice. It is therefore critical to constrain the role of geothermal flux in mobilizing ice from the interior through speed up and expansion of tributaries since interior ice has high potential for sea level change.

Along the coast, basal sliding is the dominant flow mechanism and elevated heat flux is produced by basal friction, reducing the impact of geothermal flux on ice temperature (Pollard and DeConto, 2005; Larour et al., 2012). In these areas, thermal heat fluxes can reach an order of magnitude higher than that expected for geothermal flux; also, once the pressure melting point is reached at the ice bed, any surplus of heat from geothermal flux will be absorbed by the latent heat of fusion of ice (Engelhardt, 2004b).

However, through a combination of channelized and distributed subglacial water systems, melt water produced in regions of high geothermal flux is trans-

5

ported to distal areas. In this way, geothermal flux can affect the flow of ice stream further downstream. That is, geothermal flux can indirectly enhance ice flow in coastal regions as well, through the supply of melt water that further lubricates the bed and allows sliding.

Current estimates of geothermal flux have many limitations. Ice borehole data coverage is limited and therefore not representative of large regions. In addition, this type of measurement only provides a minimum bound on geothermal flux since basal melting, if present, would reduce heat conduction into the overlying flowing ice (Engelhardt, 2004b). Indirect measurements of geothermal flux through interpretation of geophysical data allows data coverage over large regions. Two methods are currently adopted in Antarctica, one uses seismic shear velocity structure as a proxy for geothermal flux (Shapiro and Ritzwoller, 2004), the other method uses the Curie depth inferred from the frequency content of satellite magnetic data (Fox Maule et al., 2005). The two methods show conflicting results, have limited resolution and ignore the role of the upper crust in distributed geothermal flux (Figure 1.2).

One example of poorly assessed geothermal flux estimates in West Antarctica is the WAIS ice divide core site. The WAIS ice divide was selected as an ice coring site for its low basal roughness and thick ice column to drill what was believed to be a long and undisrupted ice core record covering $\sim$100 ka (Morse et al., 2002). However, only about half of that age record was actually collected at WAIS divide. Elevated geothermal flux in the range of 120-220 mW/m$^2$ (2-4 times continental average) has been estimated from borehole measurements to account for the

missing ice in the core (Fudge et al., 2012, Cuffey personal communication). Better estimates of the distribution and amplitude of geothermal fluxes are therefore critical to guide future ice core site selection for old ice targets.

## 1.2   West Antarctic Ice Sheet

Thwaites and Pine Island Glaciers flow from the WAIS ice divide towards the Amundsen Sea Embayment coasts of the Amundsen embayment while the Siple Coast's ice streams (Mercer, Whillans, Kamb, Bindshadler, and MacAyeal) drain ice toward the Ross Sea Embayment (Figure 1.1).

Thwaites Glacier is one of the largest, most rapidly changing glaciers on Earth and currently at risk of rapid collapse (Mouginot et al., 2014). Its landward sloping bed reaches into the deep interior of the WAIS, making it a main component in scenarios of rapid deglaciation (Bamber et al., 2009).

On the other hand, the Siple Coast and its five ice streams represent a very different system. Compared to Thwaites, the Siple Coast's ice streams are characterized by complex dynamics due to the strong interplay between adjacent ice streams and by lower driving stresses due to lower surface slopes. Because of the low driving stresses and the lack of strong topographic bed control, the presence of basal water is essential to sustaining ice flow through basal sliding. The low driving stresses of the Siple Coast allow thinning of the ice streams and reduced basal shearing, both of which act to cool the bed and promote freezing (Christoffersen et al., 2014). This configuration requires a large supply of subglacial water from the interior to mobilize the ice. Any fluctuation in water supply from the tributaries

7

can cause the thin ice streams to stagnate through rapid freeze-on at their bases.

Despite their differences, the setting and configuration of Thwaites and Siple Coast's ice streams will both be largely affected by heterogeneous geothermal flux and the resulting generation/availability of basal melt water.

## 1.3 West Antarctic Rift System

The WAIS flows into the West Antarctic Rift System (WARS), a Jurassic to Cenozoic intracontinental extension zone characterized by active subglacial volcanism (Blankenship et al., 1993; Behrendt et al., 1998; Corr and Vaughan, 2008; Lough et al., 2013) and elevated geothermal flux (Fudge et al., 2012; Schroeder et al., 2014a). Crustal thickness varies along the WARS, with the thickest crust being under the Siple Coast (Chaput et al., 2014). A recent study by Schroeder et al. (2014a) showed that the Thwaites Glacier catchment has an average geothermal flux of 114 mW/m$^2$ with areas of high flux exceeding 200 mW/m$^2$. These results are consistent with hypothesized rift-associated magmatic migration and volcanism (Lough et al., 2013).

### 1.3.1 West Antarctic tectonic history

West Antarctica is comprised of WARS and five crustal blocks with Paleozoic basement: Ellsworth-Whitmore Mountains (EWM), Antarctic Peninsula (AP), Thurston Island (TI), eastern Marie Byrd Land (eMBL), and western Marie Byrd Land (wMBL, Dalziel and Elliot (1982); Pankhurst et al. (1998); Curtis (2001); Luyendyk et al. (2001). In its Gondwana configuration, the five crustal blocks plus

the two that become New Zealand were grouped into two provinces with shared geochemical, paleomagnetic, and geologic signature: the Amundsen and Ross embayments (DiVenere et al., 1995; Bradshaw et al., 1997; Pankhurst et al., 1998).

### 1.3.1.1 Mesozoic times: Late Triassic to Cretaceous

Extensive studies in the western Marie Byrd Land Ford Ranges (Siddoway (2008) and references therein) provide the best Antarctic record of activity along the Phoenix (proto-Pacific) subduction zone during Gondwana breakup. Prior to ~100 Ma, active subduction along the margin produced widespread calc-alkaline magmatic arc rocks (Pankhurst et al., 1998; Mukasa and Dalziel, 2000; Dalziel and Lawver, 2001; Siddoway, 2008) while drawing the Phoenix-Pacific spreading ridge toward the subduction zone. Emplacement of Median Batholith in New Zealand occurred from 145-120 Ma (Bradshaw, et al., 1997; Siddoway, 2008) and similar plutonism has been suggested to continue throughout the Amundsen Province (eMBL, TI, and AP) from 124-96 Ma (Bradshaw et al., 1997; Luyendyk et al., 2001; Siddoway, 2008).

By 115 Ma, the young, hot, and buoyant crust of the Phoenix plate was being subducted beneath western Marie Byrd Land, raising the temperature and pressure of the lower crust to ¿800C and 7 kbar (Siddoway, 2008). These conditions initiated wide-spread metamorphism and started ductile flow in the lower crust, creating the migmatized gneiss dome now exhumed in the Fosdick Mountains, west Marie Byrd Land (Siddoway, 2008). By 110 Ma Antarctica was in the last stages of break up and had drifted into a stable polar position (Dalziel and Lawver, 2001).

9

From 105-92 Ma, a shift in the character of magmatism along the Ross Province occurred from arc magmatism to bimodal, back-arc rifting (Siddoway, 2008) followed by widespread rifting and opening of the Ross Sea (Luyendyk et al., 2001; Siddoway, 2008). The cause of the widespread Cretaceous rifting could be the start of continental rifting between Australia and East Antarctica just to the west of the now Ross Sea (Siddoway, 2008), impingement of a plume (Behrendt et al., 1991; Storey et al., 1999; Siddoway, 2008), or slow-down of subduction due to the buoyant Phoenix plate crust (Luyendyk et al., 2001). The Ross Sea continental crust is thought to have been between 40 and 50 km thick prior to the onset of rifting ($>$105 Ma) and subsequently thinned by half, though it did not yet have its characteristic ridge-trough bathymetry (Decesari et al., 2007). Despite immature bathymetry, there is evidence for syn-rifting and post-rifting sediment deposition up to several kilometers thick, which was significantly eroded later (Luyendyk et al., 2001). Since extension in the Ross Sea was $<$50 km after the start of seafloor spreading between New Zealand and Marie Byrd Land (Lavwer and Gahagan, 1994), several hundred kilometers of extension (DiVenere et al., 1995) were accomplished during a period of time only 31-22 million years long (Luyendyk et al., 2001; Eagles et al., 2004). This was a key episode of rifting because it accounts for up to 1.2x106 km$^2$ of extended continental crust across the continent (including the now ice-covered portions) and translated western Marie Byrd Land to its current location (Siddoway, 2008). The NE limit of widespread rifting outside the Ross Sea is either in the Amundsen or Bellingshausen Seas (LeMasurier and Landis, 1997; LeMasurier, 2008).

10

A separate event at ∼83-78 Ma commenced the separation of New Zealand from Marie Byrd Land and caused ocean floor spreading (Lavwer and Gahagan, 1994; Luyendyk et al., 2001; Eagles et al., 2004; Siddoway, 2008). The presumed catalyst of this event, which cut through bedrock to rift away New Zealand, is the subduction of the Phoenix-Pacific spreading ridge. This event changed the plate boundaries on both sides of the Antarctic-Pacific margin, causing seafloor spreading offshore of the eastern Ross Sea and Marie Byrd Land, as well as the creation of a Bellingshausen plate outboard of the current Amundsen Sea Embayment (Eagles et al., 2004).

### 1.3.1.2 Cenozoic times

Late Cenozoic volcanism in Marie Byrd Land (and possibly in the interior rift and Transantarctic Mountains) may have exploited old lithospheric weaknesses (LeMasurier, 1990; Blankenship et al., 1993; Dalziel and Lawver, 2001) and been generated by a plume (Behrendt et al., 1994; Van der Wateren et al., 1999), which is supported by geochemical analyses of Cenozoic volcanics Wörner (1999). The Marie Byrd Land dome, based on volcanic rocks overlying a regional erosional surface, began to rise at 28-26 Ma at a rate of about 100 m/Ma (LeMasurier and Landis, 1997). Volcanism in Marie Byrd Land started around the time of dome uplift (28-30 Ma) but its main phases of activity based on the exposed rocks occurred from 8-12 Ma and 0-1 Ma, though older Cenozoic rocks are likely more abundant and simply obscured by the current ice sheet (LeMasurier, 1990). Subglacial volcanoes (both active and dormant/eroded, (Blankenship et al., 1993; Behrendt et al.,

2004; Lough et al., 2013)) and potentially extensive amounts of flood basalts exist in the rift area beneath the Ross Sea Embayment (Behrendt et al., 1994) and could be related to the hypothesized Marie Byrd Land plume but there are few to no age constraints on their creation, other than indications that they were erupted subaerially or subglacially (Behrendt et al., 1995).

Several lines of evidence support the hypothesis that continental extension is no longer active at present. A drape of subglacial sediments across rift features in the Ross Sea Embayment indicates that they were not substantially reactivated in the Cenozoic (Blankenship et al., 2011a; Studinger et al., 2001). Magnetotelluric profiling and seismic results near the boundary between the rifted Ross Sea Embayment and the Ellsworth-Whitmore Mountains crustal block suggest cool mantle temperatures and thus no Cenozoic extension (Wannamaker et al., 1996; Clarke et al., 1997). GPS-measured motion between East and West Antarctica do not exceed the measurements noise level of 1-2 mm/yr, inferring that rifting in both the Ross Sea Embayment and the Ross Sea is very slow (or inactive) and that volcanism observed there is due to mantle upwelling, not rifting (Donnellan and Luyendyk, 2004). The current continental crust of West Antarctica, after all the phases of magmatism and rifting, is topographically mostly below sea level and has significantly thinner than average crustal thicknesses (i.e. <35-40 km).

## 1.4   Airborne geophysical datasets

Airborne geophysical data collected in West Antarctica provide extensive data coverage and enough resolution to overcome the limits of previous geothermal

12

flux estimates. Also, combining multiple types of airborne data allows the investigation of the role of the upper crust (i.e. topography and lithology) in estimates of geothermal flux.

The University of Texas Institute for Geophysics (UTIG) has collected several large radar sounding datasets in this region, including both incoherent and coherent data (Figure 1.3). *Incoherent* radar data is collected by systems that can only sample amplitude variations in the returning echo, and not the faster phase variations of the carrier frequency. Although the incoherent radar has these ambiguities, there is still a lot of information about the geometric and material properties of the bed to be exploited. *Coherent* radar data can sample the carrier frequency scale variations, allowing for rejection of scattering noise through coherent integration, as well as faster phase variations of the carrier frequency. We first focus on the older incoherent datasets in the Ross Sea Embayment, and then focus on later coherent radar sounding datasets collected with the High Capability Airborne Radar Sounder (HiCARS; (Peters et al., 2005a, 2007a; Schroeder et al., 2013)).

### 1.4.1 CASERTZ

The 1991-1997 Corridor Aerogeophysics of the South Eastern Ross Transect Zone (CASERTZ) project conducted 5 km x 5 km grids over the onset regions of the Siple Coast Ice Streams from Willians Ice Stream to the Ross - Amundsen Divide, including the entirety of Bindschadler Ice Stream (Blankenship et al., 2001). The project used one of the first GPS-enabled Twin Otter aircraft instrumented with a gravimeter, magnetometers, laser altimeters, and a digital version of an incoher-

Figure 1.3: Radar datasets over West Antarctica. CASERTZ (Blankenship et al., 2001) and related incoherent radar surveys are in purple; the coherent AGASEA data studied in Schroeder et al. (2013, 2014a) are in black over Thwaites Glacier; unevaluated AGASEA, ATRS (Peters et al., 2005b) and GIMBLE flightlines are in orange over the interior and the Siple Coast. Background shading is ice sheet velocities (Rignot et al., 2011b). Grounding line is shown with a solid black.

14

ent analog radar system developed by the Technical University of Denmark (TUD), first flown in the 1970's as part of a joint NSF-Scott Polar Research-TUD effort. This system (referred to here as the TUD system) operated at 60 MHz with a pulse width of 0.25 $\mu$sec. The pulse repetition frequency (PRF) was 12 kHz, with each returned pulse being rectified and log-detected to provide amplitude, then averaged over 0.25 seconds. The result was a system with high dynamic range, but high sensitivity to scattering noise. Reflection analysis using this system in the interior of East Antarctica can be found in Carter et al. (2007) and Carter et al. (2009), however, the complex environment of the West Antarctic Ice Sheet requires augmenting coherent data to conduct the complete evaluation of the underlying hydrology, required to infer geothermal flux.

### 1.4.2 HiCARS

HiCARS is a coherent, 60 MHz center frequency, 15 MHz bandwidth high-power radar sounder which as been operated in various versions for the last 14 years by UTIG. The system operates with a PRF of 6400 Hz, which is stacked 16 or 32 times prior to recording to yield coherent traces at 200 Hz. This high record rate allows HiCARS to fully sample the full Doppler bandwidth and perform subsurface along-track SAR focusing, along-track Doppler based clutter discrimination, and characterize the along track scattering function of the bed. Two channels separated by gain allow for simultaneous measurement of surface and bed echoes across a dynamic range of 120 dB.

The full HiCARS system was first flown on a Twin Otter during the 2001

15

field season (Peters et al., 2005a; Holt et al., 2006b; Peters et al., 2007c,b), during the 15-flight Advanced Technology Radar Sounder (ATRS) program operating in the Ross Embayment. Targeted lines were flown over the divide, the Bentley Subglacial Trench, Bindschadler Ice Stream and Kamb Ice Stream. HiCARS was then deployed for the Airborne Geophysics of the Amundsen Sea Embayment (AGASEA) project for a systematic survey of Thwaites Glacier (Holt et al., 2006a; Young et al., 2008; Diehl et al., 2008; Schroeder et al., 2013, 2014a). An orthogonal 15 X 15 km grid was flown over the entire New Mexico sized catchment. HiCARS 2, a similar system with upgraded components, was flown over the upper MacAyeal Ice Stream at 5 km line spacing as part of the Geophysical Investigations of Marie Byrd Land Evolution (GIMBLE) aerogeophysical project.

# Chapter 2

# Tectonic and thermal evolution of the West Antarctic margin under Thwaites Glacier from aeromagnetics

## 2.1 Introduction

The West Antarctic Ice Sheet (WAIS) sits on top of the West Antarctic rift system (WARS), a Cretaceous through Cenozoic region of extended crust and active volcanism that imposes a unique set of boundary conditions to the overlying ice sheet. WARS' characteristic low and cradle-shaped topography makes WAIS the largest marine ice sheet on Earth. In addition, WARS' active volcanism and elevated geothermal flux can potentially generate large quantities of melt water that can lubricate the ice-bed interface and facilitate fast ice flow. WARS' geological evolution is key to understanding the distribution of regions of older and likely colder crust and areas of more recent tectonic activity, likely to be warmer and volcanically active.

WARS began to form during the break up of Gondwanaland in the mid-Mesozoic (Storey et al., 1988; Van der Wateren and Cloetingh, 1999). Two major phases of WARS extension have been hypothesized, the first one in the Jurassic-Cretaceous, which accommodated most of the intracontinental extension; and the second one in the Cenozoic, which initially affected the Ross Sea region and then

17

regions further inland, and emplaced bimodal alkali volcanic rocks later in the Miocene (Behrendt, 1999; Karner et al., 2005; Wilson and Luyendyk, 2006). However, uncertainty still exists on the timing and evolution of WARS due to WAIS' extensive ice cover and consequent limitation on number of geological and geophysical studies in the area.

Here we show evidence for three distinct magnetic provinces within northern WARS, which supports the hypothesis that WARS experienced multi-stage extension and different mantle regimes, reveal the spatial extent and geological manifestation of subsequent stages of extension, and explain the distribution of active subglacial distribution in WARS' geological context.

## 2.2    Geological background

At the start of the Gondwana supercontinent breakup and subsequent development of the southern oceans, about 200 Ma, West Antarctica consisted of seven discrete microcontinental blocks that moved relative to one another and to the East Antarctic craton (Fig. 2.1): Ellsworth-Whitmore Mountains; Antarctic Peninsula; Thurston Island; eastern Marie Byrd Land; western Marie Byrd Land; and the Chatham Rise and Campbell Plateau, which then became New Zealand. The stages of extension, and subsequent separation, of New Zealand from the Antarctic Plate dominate the tectonic signature of the Pacific margin of West Antarctica. Early divergence of the Pacific and Antarctic plates began as early as 90 Ma with rifting and crustal extension between Chatham Rise and easternmost Marie Byrd Land (Eagles et al., 2004; Larter et al., 2002; Wobbe et al., 2012) (Fig. 2.2a). By 84-83

18

Ma, this early rifting was abandoned in favor of the formation of a new extensional ridge between the Campbell Plateau and Marie Byrd Land, which led to the formation of the earliest oceanic crust offshore of Marie Byrd Land (Fig. 2.2b). Starting around 79 Ma, the Bellingshausen Plate began to move independently of the Pacific and Antarctic Ridge until about 61 Ma (Fig. 2.2c,d). The Bellingshausen Plate's western boundary passed through the region of the Marie Byrd Seamounts, north of the Amundsen Sea Embayment. Its eastern transpressional boundary lies along the Bellingshausen Gravity Anomaly lineament in the western Bellingshausen Sea (Eagles et al., 2004; Gohl et al., 1997).

## 2.3   Magnetic survey and data processing

The region comprising eastern Marie Byrd Land and Thwaites, Smith, Kohler, Pope, and Haynes Glacier catchments was the target area of the 2004/2005 Airborne Geophysics of the Amundsen Sea Embayment, Antarctica (AGASEA) aerogeophysical campaign (Holt et al., 2006a; Young et al., 2008). Aeromagnetic data were collected along with ice surface elevation, ice thickness, subglacial bed elevations, and airborne gravity data on a 15 x 15 km flight grid using a Twin Otter aircraft configured and operated by the University of Texas Institute for Geophysics (UTIG) (Fig. 2.3a,b). Aeromagnetic data were acquired with a Geometrics Cesium Vapor magnetometer towed behind the aircraft and recording at 10 Hz sample rate. Aeromagnetic data were analyzed following standard data reduction processing. Diurnal variations of the geomagnetic field were corrected for using data from stationary magnetometers operated at two base stations, at Thwaites and Pine Island

19

camps. Aeromagnetic data were levelled, draped (Pilkington and Thurston, 2001) onto the subglacial topography at a distance 3200 m above the bedrock, and gridded with a minimum-curvature algorithm (1000 m grid mesh). No rotation to pole was applied since the magnetic inclination in the study area is $69\pm1°$. The AGASEA aeromagnetic dataset was collected at a time of anomalously intense geomagnetic activity, culminated in the solar storm of January 2005. This resulted in disturbance during acquisition which affected data quality. However, after data processing the final crossover analysis of the magnetic anomalies yielded a 13.5 nT RMS error, which is well within the resolution of interest for this study.

## 2.4 Results

### 2.4.1 Magnetics

We identify three regions characterized by different magnetic anomaly fabric (Fig. 2.3c). The first region, named Thwaites Magnetic District (TMD) is located along the main tributary of Thwaites Glacier. It consists of positive (300-700 nT), elongated, and sub-parallel magnetic anomalies with a ENE-WSW orientation. The second region, Marie Byrd Land Magnetic District (MMD) is located between THW and eastern Marie Byrd Land (eMBL). MMD consists of relatively low amplitude (50-200 nT) and high frequency magnetic anomalies. The third region, Pine Island Magnetic District (PMD) runs along the catchments between THW and Pine Island Glacier (PI). This region is characterized by positive (300-700 nT), circular magnetic anomalies with radius between 50 - 200 km, most of which show a magnetic low at the center.

### 2.4.2 Bed topography

The bed topography underneath magnetic districts TMD and PMD is mostly below sea level (up to -1500 m) (Fig. 2.3b). In TMD, WARS' bed topography from Goff et al. (2014) shows a smooth bed, especially underneath each major tributary of THW. PMD on the other hand shows a generally rougher and more varied bed topography. The bed topography in MMD is largely above sea level ($\sim$1000 m) and characterized by a set of sub-parallel valleys oriented ENE-WSW (Fig. 2.3d).

## 2.5 Discussion

The linear magnetic anomalies in TMD parallel the set of elongated magnetic anomalies oriented ENE-WSW interpreted by Gohl et al. (2013) off shore from THW, in the Amundsen Sea (red lines in Fig.2.3c,d). The ENE-WSW trending anomalies parallel the azimuth of the initial spreading center between CR and the Antarctic Plate, along the northern margin of THW, and have been related to rift processes occurring before and during break up, between 100 - 85 Ma (Fig. 2.2a). Gohl et al. (2013) interpret the ENE-WSW trending anomalies as wedges of mafic intrusions of the kind typical of volcanic extended continental margins (Planke and Eldholm, 1994; Wolfenden et al., 2005). We interpret the magnetic lineaments in TMD as the inland continuation of the original Cretaceous rift fabric observed offshore of THW by Gohl et al. (2013). THW's grounding line is currently anchored to crystalline rock, interpreted from gravity anomalies (Diehl et al., 2008), that also corresponds to one of our interpreted elongated magnetic anomalies.

The elongated ENE-WSW oriented magnetic anomalies do not propagate into the adjacent magnetic districts. However, the presence of similarly oriented incised valleys in MMD (Fig. 2.3d) suggests a potential tectonic structural control in valleys formation. We interpret MMD as a region tectonically related and affected by the original Cretaceous rift between CR and the Antarctic Plate (Fig. 2.2a) and explain the lack of rift-related elongated magnetic anomalies due to later stages of margin reactivation both in the Cretaceous and Miocene.

A new spreading ridge between CP and the Antarctic Plate, along the northern margin of eMBL, initiated around 80 Ma (Fig. 2.2b). Rift processes before and during the break up of the CP could have triggered decompression melting within the fertile mantle wedge formed during the long lived subduction of the Phoenix plate under the Antarctic plate. Hydrothermal alteration destroys the magnetic susceptibility of minerals in volcanic rocks and as has been observed to remove magnetic anomalies (Finn and Morgan, 2002; Hochstein and Soengkono, 1997). We suggest that eMBL is an area of the rift that has undergone crustal reheating and hydrothermal alteration, which led to loss of the original magnetic character.

Alternately enhanced heating can rise the Curie point within the crust and suppress long wave magnetic anomalies, as all rocks are nonmagnetic once they reach the Curie temperature (Turcotte and Schubert, 2014). However, using a basalt wedge 10 km thick as modeled by (Gohl et al., 2013) and assuming that the Curie temperature is reached within 2 km of the rock-ice interface, the geothermal flux needed to erase the rock's magnetism would exceed $600 \ mW/m^2$, which is unreasonable. Based on these results, the demagnetization of eMBL is more consistent

with being the result of pervasive hydrothermal alteration (Finn and Morgan, 2002). Additional re-heating, hydrothermal alteration, and loss of magnetic signature in MMD can be related to the impingement on the lithosphere of a hotspot (LeMasurier and Rex, 1989) which resulted in the uplift of MBL, currently up to ∼1000 m above sea level.

POLENET's estimates of crustal thickness, seismic anisotropy, and lithosphere elastic properties in West Antarctica (An et al., 2015; Chaput et al., 2014; Accardo et al., 2014; Lloyd et al., 2015) detected a gradient in crustal thickness within WARS, with thinner crust in the lineament and circular anomaly magnetic districts (TMD and PMD), and thicker crust in the low amplitude and high frequency magnetic district (MMD). These results are consistent with our interpretation that TMD and PMD correspond to rifted, stretched out crust targeted by Cretaceous syn- to post- rift volcanism and caldera formation, while in MMD, crustal thickening can be explained by multiple stages of magmatic accretion of the upper crust due to rift-related decompression melting in the Cretaceous and impingement of a hotspot on the lithosphere in the Cenozoic. The hotspot hypothesis is also supported by the pattern of radial seismic anisotropy detected in MMD, which superimpose the main rift-axis parallel seismic anomaly observed in West Antarctica(Accardo et al., 2014) and by evidence of a regional negative Bouguer disturbance in MBL (Damiani et al., 2014), consistent with a low-density upper mantle.

Around 79 Ma, the newly formed Bellingshausen Plate started to rotate with respect to the Antarctic Plate (Fig. 2.2c). The complex pattern of rotation induced both transcompression and transtension stress patterns along the plates margins (Ea-

gles et al., 2004). The movement of the Bellingshausen Plate could explain the production of melt and the onset of a transtentional stress regime that accommodated the formation of calderas in PI. We interpret the circular anomalies in PMD as an area of volcanic activity and caldera formation within the extensional crustal regime generate by the Bellingshausen Plate rotation motion.

## 2.6   Conclusions

We derived magnetic anomalies from the AGASEA aeromagnetic dataset in West Antarctica using standard data reduction techniques (Fig. 2.3a). Analysis of the magnetic anomalies reveal complex patterns in the magnetic fabric. We identify three distinct magnetic districts (Fig. 2.3c): TMD over THW's main trunk is characterized by high (300-700 nT) positive elongated magnetic anomalies which we interpret as mafic intrusions emplaced during the mid-Cretaceous rifting between CR and the Antarctic Plate; PMD in the PI region is characterized by positive, high (300-700 nT) donut-shaped anomalies. We interpret this as a region of transtensional stress and caldera formation related to the complex rotation of the Bellingshausen Plate in the late Cretaceous. Finally MMD in eMBL shows low amplitude (50-200 nT), higher frequency magnetic anomalies. We interpret MMD as a region affected by the mid-Cretaceous rifting, which resulted in faulting, heating, and thickening of the crust through magmatic underplating, and was later reactivated in the Miocene by a hotspot that elevated the bed topography and further erased the original rift-related magnetic signature. Our results suggest that the most recently tectonically active regions, and likely the ones with potentially higher geothermal

24

flux anomalies, correspond to MMD and PMD.
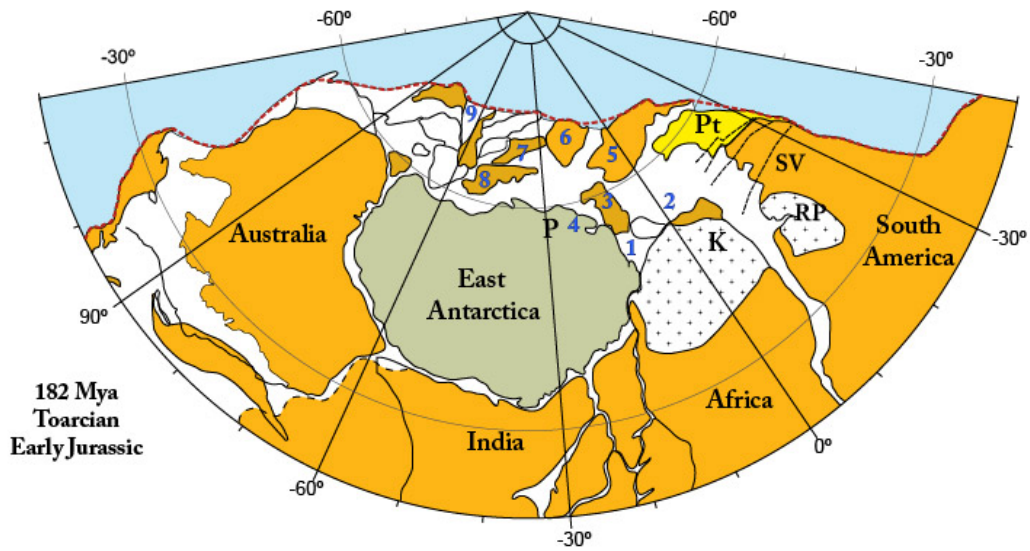
Figure 2.1: Reconstruction of the Gondwana supercontinent in Early Jurassic times (182 Mya). Precambrian cratons referred to in text are shown in gray. Pacific margin crustal units: (1) Maurice Ewing Bank, (2) Falkland/Malvinas (Lafonian) microplate, (3) Ellsworth-Whitmore Mountains crustal block, (4) Berkner Island, (5) Antarctic Peninsula, (6) Thurston IslandEights Coast crustal block, (7) Eastern Marie Byrd Land block, (8) Western Marie Byrd Land block, and (9) Zealandia (shape reconstructed to 182 Mya). Patagonia (south of the North Patagonian massif) is shown in yellow. Major continents positioned using seafloor spreading data and PLATES software of the Institute for Geophysics, The University of Texas at Austin. Abbreviations: K, Kalahari craton; M, Madagascar; P, Pensacola Mountains; Pt, Patagonia; RP, Rio de la Plata craton; SV, Sierra de la Ventana. Modified with permission from Dalziel et al. (2013).
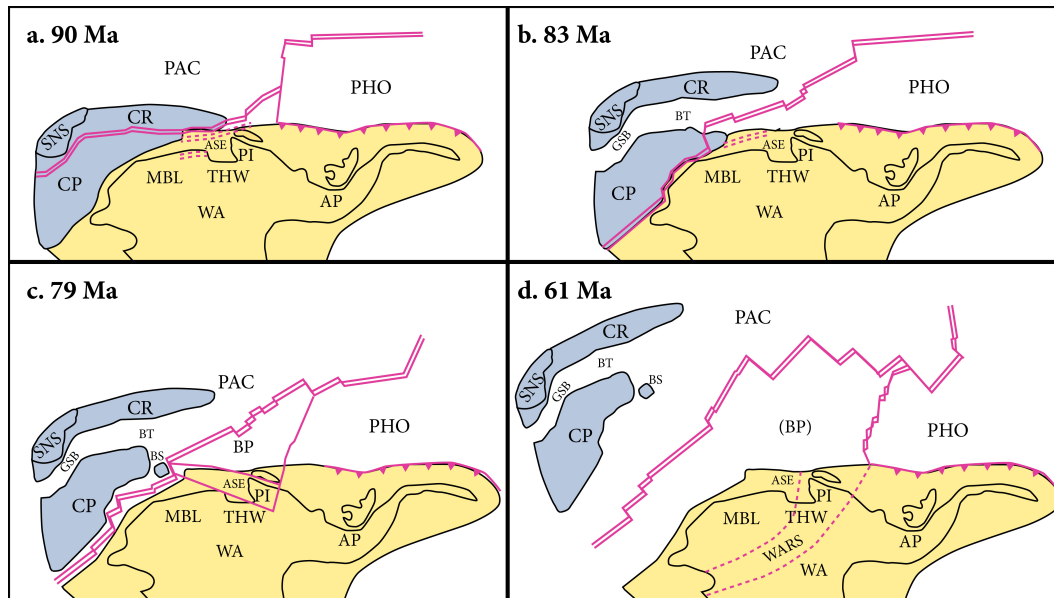
Figure 2.2: Plate tectonic reconstruction of the tectonic development in the Amundsen Sea area from 90 to 61 Ma. The plates are rotated according to rotation parameters compiled and derived by Eagles et al. (2004). Abbreviations are: AP Antarctic Peninsula, ASE Amundsen Sea Embayment, BP Bellingshausen Plate, BT Bounty Trough, BS Bollons Seamount, CP Campbell Plateau, CR Chatham Rise, GSB Great South Basin, MBL Marie Byrd Land, PAC Pacific plate, PHO Phoenix Plate, PI Pine Island Glacier, SNS South Island New Zealand, THW Thwaites Glacier, WA West Antarctica, and WARS West Antarctic Rift System. Dashed pink outline: estimated location of WARS' boundaries. Modified from Gohl et al. (2013).
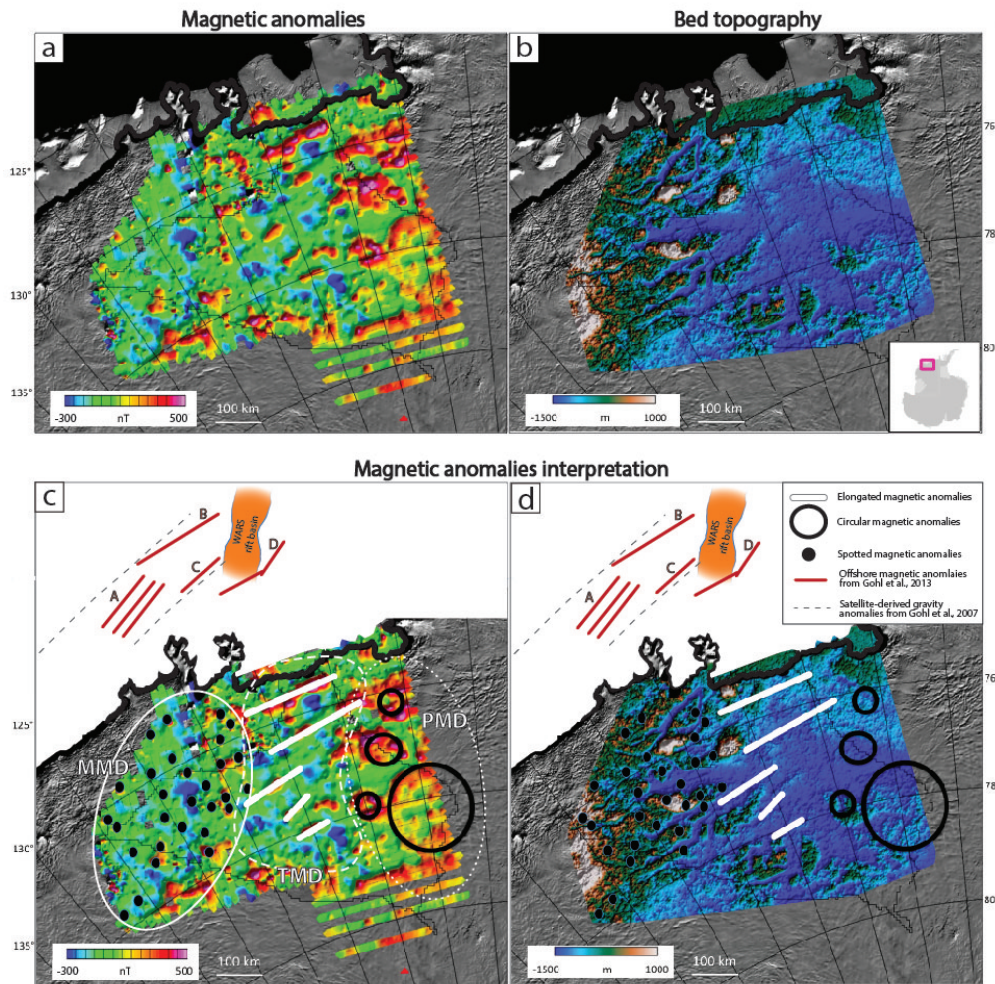
Figure 2.3: a: Magnetic anomalies; b: bed topography (Goff et al., 2014); c: interpretation of magnetic anomalies and magnetic districts identified in this study (outlined in white). MMD thin solid line; TMD dashed line; PMD dotted line. The offshore ENE-WSW trending magnetic anomalies from Gohl et al. (2013) are shown as red lines and correspond to the family of magnetic anomalies A-D in (Gohl et al., 2013); d: magnetic anomalies interpretation over Goff et al. (2014) bed topography. The ENE-WSW topographic valleys in MMD are interpreted as structural continuations of the ENE-WSW magnetically defined structures (thick white lines) in TMD. The offshore WARS rift basin (orange) is interpreted as a branch of the West Antarctic Rift System (Gohl et al., 2013). In all panels: MODIS surface images in background; thick black line shows location of the grounding line.

28

# Chapter 3

# Controls on the observed distribution of active subglacial volcanism in Antarctica

## 3.1 Introduction

Preserved within the depths of the Antarctic ice sheet lie the record of past volcanic eruptions. This record gives us the unique capacity to understand the periodicity of volcanic eruptions at a continental scale, something rarely achieved in other terrestrial environments due to record loss from weathering and limited availability of written documentation.

In West Antarctica, the dynamic marine West Antarctic Ice Sheet (WAIS) is preserved pinned to the number of subaerial volcanic edifices and chains visible throughout the region, but destabilized by the presence of the large continental West Antarctic Rift System (WARS) (Pollard and DeConto, 2009; Weertman, 1974), a region of thinned crust mostly below sea level characterized by large local mantle thermal anomalies (Chaput et al., 2014; Lloyd et al., 2015) and elevated geothermal flux (Schroeder et al., 2014a; Fisher et al., 2015; Clow et al., 2012). The potential threat that volcanism poses to WAIS' stability motivated extensive efforts to characterize subglacial active volcanism in West Antarctica (Blankenship et al., 2001; Schroeder et al., 2014a).

We hypothesize active volcanism occurs along crustal boundaries and regions of rifted, thinned crust, where local tectonic stress regimes allow for the upwelling of magma and hydrothermal fluids. We also hypothesize active volcanism will concentrate around regions of WAIS that experience large excursions in ice thickness during glacial and interglacial cycles. There, changes in ice load can cause decompression melting and magma production in the underlying mantle.

In this chapter we discuss the occurrence of active subglacial volcanism in the context of WAIS' glaciological regimes and WARS' geological and topographic structure. We concentrate on subglacial active volcanism in West Antarctica due to the abundance of observations in this region. However, the approach to subglacial volcanism identification outlined for West Antarctic can be applied generally to other passive margins in East Antarctica to begin a systematic search for similarly active subglacial volcanoes.

### 3.1.1 WARS geological context for subglacial volcanism

The lithospheric structure of West Antarctica determines key topographic, morphological, and thermal basal boundary conditions for the stability of WAIS. Moreover, it provides insights into the distribution of active volcanism, which concentrates along crustal boundaries and transition zones where stress regimes facilitate the formation and emplacement of shallow crust magma chambers.

West Antarctica consists of the WARS and five discrete microcontinental blocks characterized by distinct subglacial bed topography, crustal thickness, and magnetic and gravity anomalies (Dalziel and Lawver, 2001; Diehl, 2008; Quartini

et al., in prep.): Ellsworth-Whitmore Mountains (EWM), Antarctic Peninsula (AP), Thurston Island (TI), eastern Marie Byrd Land (eMBL), and western Marie Byrd Land (wMBL) 3.1. Crustal block boundaries are interpreted from gravity anomalies. Gradual changes in the Bouguer anomalies from positive to negative values indicate broad zones of crustal change rather than distinct crustal boundaries and are interpreted as partially rifted transitional crust (Diehl, 2008).

WARS is a region of low bed topography and stretched continental crust (Fretwell et al., 2013; Chaput et al., 2014) characterized by an heterogeneous distribution of high geothermal flux (Schroeder et al., 2014a; Fisher et al., 2015). The low topography makes large portions of central WAIS reside below sea level (up to − 2500 m), a highly unstable configuration known as the marine ice sheet instability, that can lead to runaway grounding line retreat and ice sheet collapse (Weertman, 1974; Schoof, 2007).

On the other hand, Marie Byrd Land (MBL, composed of eMBL and wMBL) is a volcanic dome of high bed topography and thicker crust (Fretwell et al., 2013; Chaput et al., 2014) sustained by a Cenozoic hot spot in the lower mantle beneath MBL, recently imaged by seismic tomography (LeMasurier and Rex, 1989; Hansen et al., 2014; Accardo et al., 2014; An et al., 2015; Emry et al., 2015; Lloyd et al., 2015; Heeszel et al., 2016). Analysis of magnetic anomalies in eMBL shows evidence for multiple stages of tectonic reactivation in the mid-Cretaceous and support the hypothesis of a hotspot emplacement in the Miocene (Quartini et al., in prep.). Magnetic fabric interpretations also show evidence for Late-Cretaceous caldera formation in TI and WARS in the region between Thwaites Glacier and Pine Island

31
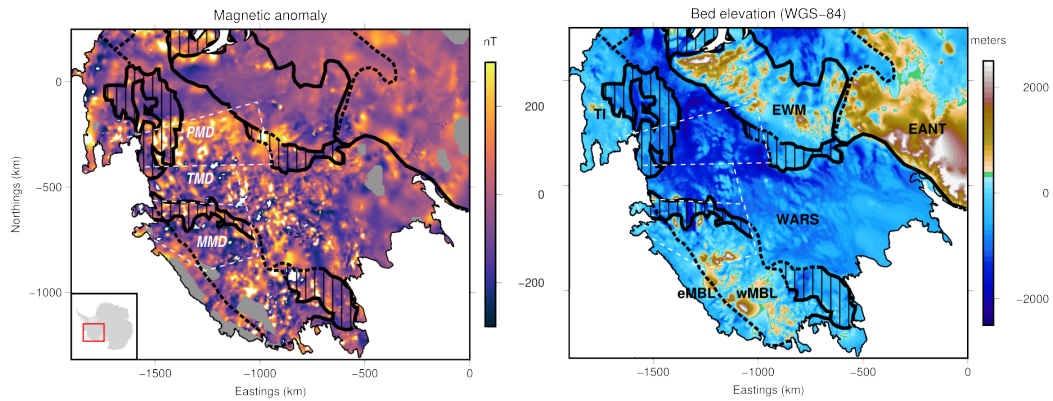
Figure 3.1: Left: ADMAP-2 magnetic anomalies (Golynsky et al., 2018). Right: BEDMAP2 bed elevation (Fretwell et al., 2013). White dashed lines outline boundaries between the Pine Island magnetic district (PMD), Thwaites Glacier magnetic district (TMD), and MBL magnetic district (MMD, Quartini et al. (in prep.)). Thick black lines outline crustal block margins and transition margins (Diehl, 2008): Thursten Island (TI), Ellsworth-Whitmore Mountains (EWM), eastern Marie Byrd Land (eMBL), western Marie Byrd Land (wMBL), East Antarctica (EANT), West Antarctic Rift System (WARS).

Glacier, and Mid-Cretaceous east-north-east West-south-west trending wedges of mafic intrusions in central WARS (Quartini et al., in prep.).

### 3.1.2 WAIS glaciological context for subglacial volcanism

The thermodynamic response of ice to pressure and temperature changes and the impact of melt water in subglacial environments introduce processes that extend the effect of volcanism both spatially and temporally. For this reason, we consider active any subglacial volcanism that has affected the current ice sheet. Based on the approximate minimum age of WAIS's oldest marine ice retrieved at WAIS divide ice core site (Buizert et al., 2015) and the cooling rates of magma chambers for compositions observed in West Antarctica (LeMasurier and Rex, 1989), we de-

fine the time interval of active subglacial volcanism in West Antarctica as the last $\sim 100,000$ years.

Geothermal flux generates basal melt water that contributes to ice sheet instability by lubricating the base of the ice sheet and causing ice streams to speed up. Basal water can facilitate sliding at the base of the ice in the area surrounding a heat anomaly and can also sustain subglacial hydraulic systems which lubricate the ice sheet further downstream (Engelhardt, 2004a; Kamb, 2001; Tulaczyk et al., 2000a; Tulaczyk et al., 2001). Therefore, the effects of geothermal flux on ice sheet dynamics are not confined to the localized area of elevated flux. Through a combination of concentrated and distributed subglacial water systems, melt water produced in regions of high geothermal flux is transported to distal areas. In this way, geothermal flux has the potential to indirectly enhance ice flow in coastal regions as well, through the supply of melt water that further lubricates the bed.

WAIS' ice dynamics and conditions at the bed impact both the type of volcanic products and their record preservation. Eruptions under thick ice generate volcanic products typical of high pressure regimes such as lava sheets and pillow lava flows (Figure 3.2 C). On the other hand, under shallower ice, volatiles in the magma expand allowing for faster quenching and breaking up of magma into hyaloclastite deposits (Figure 3.2 A). Regions of fast ice flow are more efficient at removing deposits at the bed, especially poorly consolidated material such as hyaloclastites (Behrendt et al., 1995) (Figure 3.2 B). We therefore expect ice volcanic products to be more easily removed along tributaries and ice streams and better preserved along ice divides.
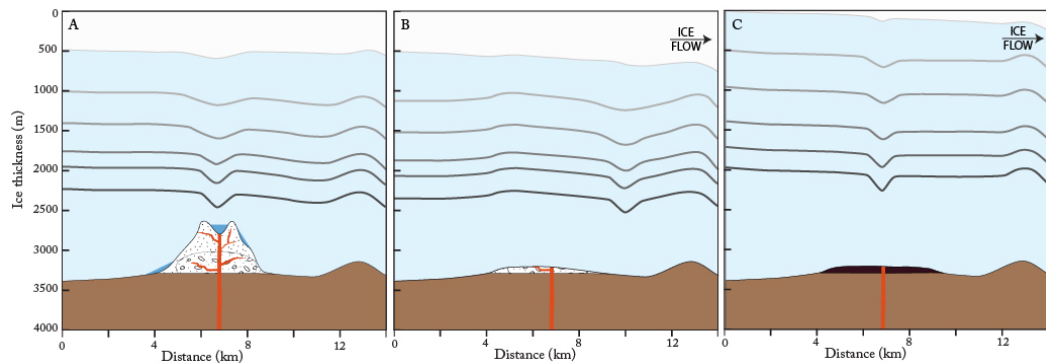
Figure 3.2: Schematic of the types of products and records of subglacial volcanic activity under different ice sheet conditions. A: poorly consolidated hyaloclastite volcanic edifice produced under shallow ice sheets; B: effect of ice removal on a hyaloclastite volcanic edifice (Nereson et al., 1998); C: erosion and removal-resistant basaltic lava flow produced under thick ice sheets.

## 3.2   Techniques and observations

Direct observations of active subglacial volcanism are difficult to obtain due to the thick West Antarctic ice sheet cover (over 2500 km thick in places). First, thick ice sheets greatly attenuate the subglacial topographic signature that can be directly inferred from the ice surface. Secondly, the single-point nature of ice cores and boreholes would make drilling efforts prohibitively expensive and overall inefficient at characterizing subglacial volcanic constructs.

Indirect observations from geophysical methods, on the other hand, provide a more cost-effective way to characterize the internal structure and properties of both the ice sheet and the underlying bed topography. Geophysical surveys have the advantage of covering much larger areas at varying degrees of spatial resolutions. Some of these methods include, but are not limited to, radar, laser altimetry,

potential fields, GPS, and passive seismic monitoring.

Identifying active subglacial volcanism requires multiple independent supporting evidence. While individual techniques can be used to identify plausible subglacial volcano candidates, it is the joint observations across different techniques and measurements that allows one to fully characterize each potential site of active subglacial volcanism. Here we will review some of the most common direct and indirect methods used to enhance the quest for active subglacial volcanism in West Antarctica.

### 3.2.1 Ice penetrating radar

Ice penetrating radar (IPR) transmits electromagnetic waves that travel through media and detect changes in the dielectric permittivity of different materials by reflecting and refracting part of their energy along each interface (Fahnestock et al., 2001). The dielectric permittivity is a property of materials that depends on composition, density, and structure. Therefore IPR can both detect the geometry and identify some properties of subglacial interfaces. The larger the contrast in dielectric permittivity of two continuous materials, the stronger the IPR reflection and easier it is to identify interfaces, also called radar reflectors.

IPR images the shape of the ice surface, bed topography, and englacial layers caused by ash and aerosol products of volcanic eruptions that become incorporated in snowfall (Fahnestock et al., 2001; Hindmarsh et al., 2006; Siegert et al., 2004b). Englacial layers are interpreted to represent isochronous events recorded within the ice (Whillans, 1976; Fujita et al., 1999; Jacobel et al., 1993). Englacial

radar layers are particularly useful as they allow geographical extension of the composition and age/depth record measured in ice cores, over hundreds of square kilometers. Evidence for active subglacial volcanism from IPR comes from interpretation of both the geometry and properties of radar interfaces.

**Geometry of radar interfaces:** Radar reflectors image the shape of the ice surface, bed topography, and englacial layers, which can provide evidence for the presence of active subglacial volcanoes in a number of ways. The subglacial bed topography can reveal volcanic constructs based on analysis of the morphology and aspect ratio of topographic reliefs. The internal structure of the ice sheet, revealed by tracing englacial layers, provides a record of changes in ice flow patterns and basal melt rates in the region. IPR data has been used to constrain melt rates through the interpretation of radar layer draw down to infer melted ice loss at the bed(Fahnestock et al., 2001). In areas of known or negligible basal friction, excessive melt production and layer draw down formation can be indicative of anomalously high subglacial geothermal flux and volcanic activity. Excessive basal melt and internal deformation in the ice column can create a depression in the ice surface called ice cauldrons, (Gudmundsson, 1996; Gudmundsson and Högnadóttir, 2007; Björnsson, 2003). Depressions in ice surface elevations can be detected by IPR or measured with higher precision (within few centimeters) by laser altimeters and used to infer areas of active subglacial volcanism (Blankenship et al., 1993).

**Properties of radar interfaces:** The most common properties of interfaces that can be extrapolated from IPR echoes are reflectivity, roughness, specularity, and anisotropy. While reflectivity is a measure of the strength of a radar

36

reflector, which is proportional to the contrast in dielectric constants between two adjacent materials, roughness and specularity are a measure of the angular spread of IPR echo returns. Roughness is calculated as the root mean square (RMS) average of the profile height deviations from the mean line, recorded within the evaluation length (Shepard et al., 2001). If the deviations are large, the surface is rough. Specularity refers to the ratio of specular over diffuse radar echo returns, where specular returns identify mirror-like surfaces that reflect waves along the same incident path, and diffuse surfaces scatter the incident wave across a wider range of angles. Water is highly specular while rock and sediments behave more like diffuse surfaces (Schroeder et al., 2016a). Specularity can be thought of as small scale roughness, or roughness calculated over a shorter evaluation length. One advantage of specularity and roughness measurements is their high insensitivity to attenuation through the ice column, which is the biggest source of uncertainty in reflectivity measurements. Finally anisotropy refers to a measure of the along track versus cross track distribution of the interface's properties. This is particularly relevant when radar surveys are planned in orthogonal grid. It can happen that one property of the interface is more apparent along one of the two acquisition directions, in which case the interface is anisotropic (Schroeder et al., 2014b; Young et al., 2015). The joint interpretation of radar interface properties can therefore inform about the properties and structure of different media.

Liquid water has much higher dielectric permittivity compared to rock, sediment, and ice. Therefore water at the ice/bed interface can be detected as a strongly reflective, smooth, and specular reflector relative to the surroundings (Gudmandsen,

1971; Peters et al., 2005a). While bed echo reflectivity and specularity have been used to detect basal water (Peters et al., 2005a; Schroeder et al., 2014a), anisotropy has been used to characterize subglacial water distribution networks (Schroeder et al., 2015).

A combination of IPR subglacial water detection and characterization techniques was used together with a subglacial water routing and glaciological model to assess melt production due to elevated geothermal flux and map active subglacial volcanism in the Thwaites Glacier catchment (Schroeder et al., 2014a). Similarly, the property of ash layers to produce highly reflective englacial layers through volume scattering has been used to map the extent of a volcanic eruption fall-out in the Hudson Mountains and identify the source subglacial volcano location (Corr and Vaughan, 2008).

**Limitations in radar interfaces interpretation:** Accurate interpretation of radar interface geometries relies on three main factors: the survey line spacing, the interpolation algorithm, and the radar acquisition system and processing technique. The spacing between survey lines impacts the final resolution of interpolation products such as Digital Elevation Models (DEM). Line spacing is a function of the survey design, usually optimized for the specific science goals of each survey. Exploratory surveys maximize areal coverage at the expense of resolution, while the opposite is true for target specific surveys. Aerogeophysical surveys can have line spacing between a few to tens of km depending on whether the survey was flown with a helicopter or fixed wing airplane respectively. Ground surveys can achieve the highest level of detail with line spacing that can vary between hundreds to a few

meters but are usually extremely target specific due to the limit in range of this kind of operations.

The interpolation algorithm applied to generate DEMs of the bed, surface, or englacial layers elevation have a number of downsides such as the use of smoothing techniques. These produce estimated curves that does not necessarily pass through all the given points, and therefore represents a conservative value for both mountains and valleys. The above mentioned limitations require any subglacial features of interest to be detected along a number of survey lines that satisfy a sufficient sampling of the geometry of the feature. The type of radar acquisition system utilized and the subsequent type of processing applied to radar data, largely impact the observed geometry of radar interfaces (Fig. 3.3). The most accurate geometries are rendered by phase-preserving coherent radar acquisition systems (such as HiCARS and HiCARS2) combined with focusing techniques that trace the energy of reflectors to their locations or origin in a radar profile. This removes hyperbolae tails in the radar echoes that would otherwise mask subglacial features such as mountains with slopes similar to or greater than the apparent slopes of the hyperbolae tails.

Limitations in both data acquisition and processing techniques can therefore fundamentally impair geometries detected by IPR and all interpolated products derived from it, ultimately invalidating interpretations. One example is the subglacial volcano catalog compiled by de Vries et al. (2017), which is based on direct interpretation of Bedmap2 bed morphology (Fretwell et al., 2013) to identify subglacial shield volcanoes. However, the large data acquisition gaps present at the time of Bedmap2 products release (e.g. in MBL) and the use of a smoothing interpolation

Comparison of airborne radar methods at Kamb Ice Stream

Incoherent acquisition
0.25 µsec pulse
60 Mhz UTIG/TUD
1993

Coherent acquisition;
coherent intergation of 320 records

Full 2-d focused SAR processing

Coherent acquisition
1 µsec chirp
0.1 µsec virtual pulse
60 Mhz UTIG/JPL/KU/TUD
2001
(Little SAR processing)
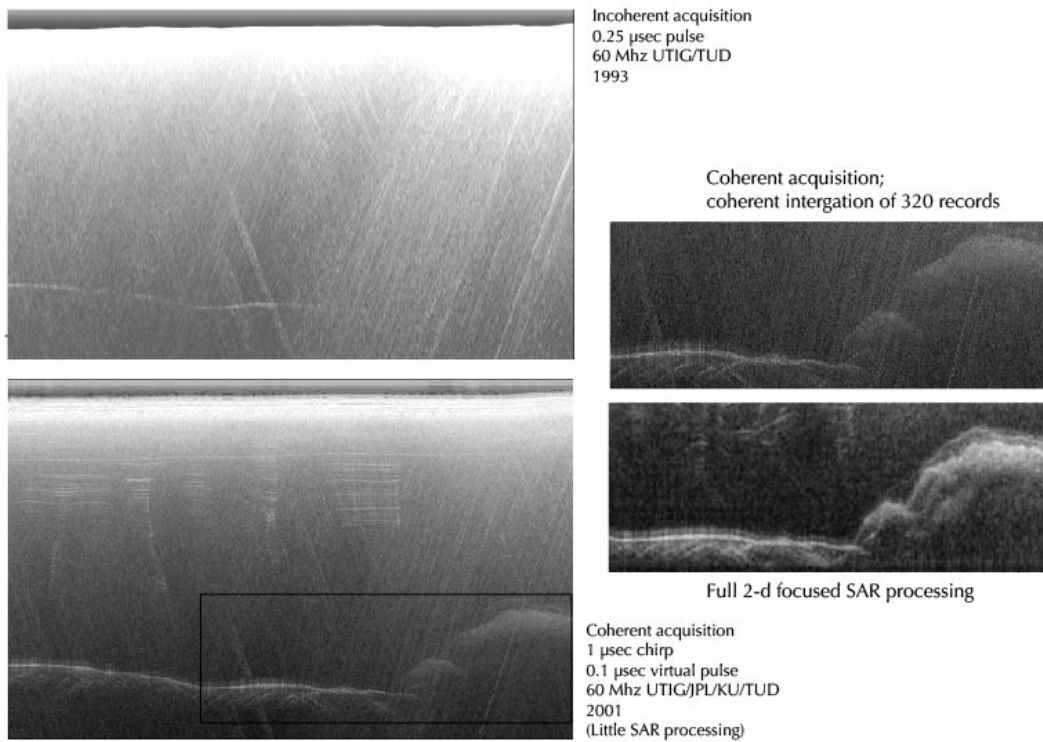
Figure 3.3: Comparison between types of radar processing and products. Upper left: incoherent radar; lower left: coherent radar. Upper right: unfocused radar; lower right focused radar.
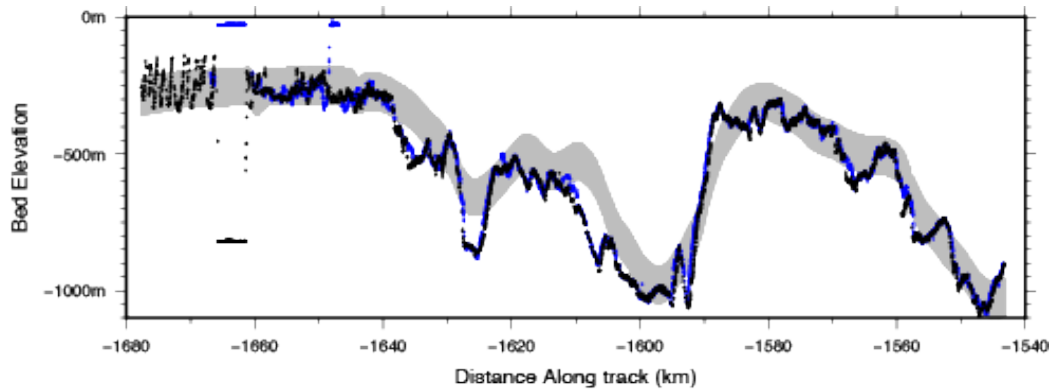
Figure 3.4: Comparison between bed elevation products along survey line THW/SJB2/X53d. Blue: bed elevation traced from unfocused radar; black: bed elevation traced from focused radar; gray: Bedmap2 bed elevation interpolation showing $\pm 67$ m uncertainty, as determined for Carson Inlet, West Antarctica (Fretwell et al., 2013).

spline generated a final bed topography DEM that deviates by hundreds of meters from the input IPR data values (Fig. 3.4).

The interpretation of layer drawdown geometry relies on the existence, persistence, and continuity of layers in radar profiles. Further, the strength of bed echoes are affected by a combination of englacial attenuation (Matsuoka, 2011) and the material and geometric properties of the ice sheet and bed, which introduce ambiguities in quantitative echo interpretation. It is important to note that the interpretation of layer drawdowns are non-unique. A number of processes unrelated to volcanic activity can similarly deform the ice column and englacial layers (Siegert et al., 2004a). Mechanical deformation due to ice flow over a subglacial obstacle, variations in vertical strain rates (Raymond, 1983), ice sheet surface slope variations due to changes in surface accumulation rates (Vaughan et al., 1999), and

41

changes in ice flow direction (Siegert et al., 2004a) deform layers in similar ways. Here we refer to anomalous layer draw downs as particular layer drawdowns the genesis of which cannot be explained by geo- or ice-dynamic processes other than melting from elevated geothermal heat. Similarly, the presence of water at the ice-rock interface is non-unique to geothermal heating nor is indicative of processes that take place in-situ, at the location where water is detected. Water melt can be produced by basal frictional heating and advected from higher hydropotential regions, therefore be representative of processes characteristic of different geological settings.

### 3.2.2 Potential fields

As gravity and magnetic field data smooth as a function of distance from the source, volcanic anomalies relating to processed at the ice-rock interface should have relatively high frequency content. However, limitations in the ability to detect volcanic constructs from potential fields data arise from the original data acquisition parameters. Both line spacing and source to sensor distance impose limits to smallest resolvable feature size and require surveys to be designed accordingly.

The character and pattern of magnetic anomalies are used to map the distribution of igneous rocks, which have high content in magnetic minerals and high magnetic susceptibility. Magnetic anomalies can be modeled with both forward and an inverse methods to define the shape and depth of the source igneous body. High magnetic susceptibility values required to simulate observed magnetic anomalies, especially when closely associated with subglacial topographic features observed

42

in radar data, are evidence for the rocks volcanic origin. The spatial pattern of magnetic anomalies is also an indication of volcanic origin and activity. Circular, "donut shaped" patterns of high amplitude magnetic anomalies surrounding central magnetic lows mark known volcanically active or young calderas, such as in Yellowstone and the Rocky Mountains area of the US (Bhattacharyya and Leu, 1975; Smith and Braile, 1994).

The magnetization of rocks is a function not only of the content of magnetic mineral, but also temperature. Both intrusive and extrusive igneous bodies must have cooled below the Curie temperature for magnetite (580 °C) to produce a magnetic anomaly. It follows that hot, molten igneous rock that are at the Curie temperature show no magnetic signature. Therefore one can expect cold igneous rocks to show a strong magnetic anomaly but hot and active areas of volcanism to have a negligible magnetic signature due to the elevated temperature of the rocks. This leads to the characteristic magnetic anomaly "donut" shape seen in active volcanic centers, showing a negligible (close to zero), low amplitude magnetic anomaly surrounded by high amplitude magnetic anomalies.

The 100,000 year limit we impose on the search for active subglacial volcanism helps us narrow the search to positive magnetic anomalies. Since the last major magnetic reversal was 780,000 years ago, negative anomalies, if due to negative remnant anomaly, should be older than 1Ma and therefore outside our interval of interest. A brief complete reversal, the Laschamp event, occurred only 41,000 years ago during the last glacial period. That reversal though lasted only about 440 years and the actual change of polarity lasted around 250 years. Mt Resnik is a

major subglacial edifice near the Bentley Subglacial Trench, which has a negative anomaly (Behrendt et al., 2006). It is unlikely that Mt. Resnik was entirely built in 250 yrs, therefore the negative magnetic anomaly of Mt. Resnik dates this volcano at more than 0.8 Ma therefore too old and too cold to have had an impact on the current ice sheet.

Joint inversions of magnetic and gravity anomalies, which detect density contrasts, are used to model the distribution of sediments and the shape and depth of igneous rocks.

### 3.2.3 Seismology

Deep long-period (DLP) earthquakes are a type of volcano-seismic activity identified in many volcanic settings including the Aleutian Islands, the Pacific Northwest of North America, Hawaii and Mount Pinatubo (Nichols et al., 2011; Okubo and Wolfe, 2008; Power et al., 2004). DLP are characterized by deep hypocenters (at or below the brittleductile transition zone), low-frequency energy ($< 5$ Hz), and swarm behavior (Okubo and Wolfe, 2008) and are hypothesized to represent the movement of magma and other fluids within volcanic and hydrothermal systems. Seismic data also reveals variability in seismic wave velocity and patterns of mantle anisotropy, which are used to image the distribution of thermal anomalies within the mantle and estimate crustal thickness. In West Antarctica, 10 permanent colocated GPS and broadband seismic stations measure relative plate motion and seismicity in central WARS as part of the Antarctic Polar Earth Observing Network (ANET-POLENET). To improve spacial coverage and produce

44

higher-resolution tomography, during the 2010-2012 campaign additional 13 temporary stations were installed across WARS between the Whitmore Mountains and Marie Byrd Land (Hansen et al., 2014; Lloyd et al., 2015; Emry et al., 2015; Heeszel et al., 2016).

### 3.2.4   Direct measurements

Direct measurements of geothermal flux via borehole thermometry are extremely difficult to undertake due to inaccessibility of the ice sheet bed. Ice borehole data coverage is also limited and therefore not representative of large regions. In addition, this type of measurement only provides a minimum bound on geothermal flux since basal melting, if present, would reduce heat conduction into the overlying flowing ice (Engelhardt, 2004a).

## 3.3   Active subglacial volcanic sectors

We group active subglacial volcano candidates into sectors based on the portion of WAIS impacted by their activity (Table 3.1). Available datasets are evaluated for evidence of active volcanism at each candidate site.

Table 3.1: Volcanic sectors

| Feature | Ice flow organization | Driving stress | Bed elevation | Crustal thickness |
|---|---|---|---|---|
| Siple Coast | Fast flowing ice streams | Low | Below sea level | Thin |
| WAIS ice divide | Low to no flow | Low to none | Below sea level | Thin |
| Marie Byrd Land | Low flow | Low | Above sea level | Thick |
| Amundsen Sea Embayment | Fast lowing ice streams | High | Below sea level | Thin |

### 3.3.1 Siple Coast sector

The Siple Coast is located within a low bed topography region of WARS characterized by relatively thin crust (Chaput et al., 2014). It is bounded by the EWM crustal block and the Transantarctic Mountains to the South and by eMBL to the North.

Subglacial volcanic activity in this region is of particular interest since subglacial melt water production sustained by elevated geothermal flux has the potential to impact ice streams dynamics along the Siple Coast. The Siple Coast's ice streams are characterized by low driving stress due to low ice surface slopes and lack of strong topographic bed control, which makes the presence of basal water essential to sustaining ice flow through basal sliding. Moreover, the low driving stresses of the Siple Coast allow thinning of the ice streams and reduced basal shearing, both of which act to cool the bed and promote freezing (Christoffersen et al., 2014). This configuration requires a large supply of subglacial water from the interior to mobilize the ice. Fluctuations in water supply can cause the thin ice streams to stagnate through rapid freeze-on at their bases.

### 3.3.1.1 Mt. CASERTZ

Subglacial volcanic activity at Mt. CASERTZ was first identified by Blankenship et al. (1993) from radar and magnetic data evidence 3.5 and later supported by analysis of englacial ash layers compatible with subglacial eruptions sourced at Mt. CASERTZ (Iverson et al., 2017). Mt. CASERTZ is located northwest of the Whitmore Mountains, in the transition zone between the EWM crustal block and the

Ross Subglacial Basin, along an ice tributary $\sim$ 100-200 km upslope of the Siple Coast's area of ice stream initiation.

In radargrams, Mt. CASERTZ shows as a cone-shaped subglacial topographic edifice about 6 km across that rises $\sim$ 650 m above the surroundings. Mt. CASERTZ stands in the central portion of a 23 km-wide caldera bounded by a rim 100-200 m in height. The cone steep slopes ($\sim$ 12°) indicates that the edifice was extruded into the ice or possibly under water before the development of the WAIS. The ice surface elevation at the location of Mt. CASERTZ's central edifice shows a 48 m deep depression. Since ice flows in the region enter the ice surface depression from the north and south, the large ice surface anomaly requires a 10-20 W/m$^2$ heat source at the base, melting $\sim$0.07 km$^3$ of ice each year, to be sustained (Blankenship et al., 1993).

The bed radar echo strength at the location of Mt. CASERTZ is weaker compared to those in areas of both equivalent and larger ice thickness in West Antarctica, indicating the ice above the central edifice is anomalously warm (Blankenship et al., 1993). This is due to the temperaturedependent dielectric attenuation of radio waves through ice to which IPR is sensitive and can detect. The bed radar echoes show tails of diffraction hyperbolae characteristic of rugged terrains (Blankenship et al., 1993). The composition of the central edifice is therefore consistent with hyaloclastite, a volcaniclastic accumulation of angular glass fragments formed by rapid cooling and fragmentation of lava flow surfaces during volcanic eruptions under water, under ice, or where subaerial flows reach bodies of water. Hyaloclastite has characteristically rough surfaces with fragments that behave like

point scatters that diffract radar waves in the same way observed at Mt. CASERTZ. Importantly, hyaloclastite is a poorly consolidated material easily eroded by ice removal (Behrendt et al. (1995), Fig.3.2. The presence of hyaloclastite therefore indicates that Mt. CASERTZ is a recently erupted volcano that has not yet suffered removal by the above ice sheet (Blankenship et al., 1993). Subglacial melt water production sustained by elevated geothermal flux at Mt. CASERTZ is supported by the presence of nearby subglacial lakes, indicated by bright and flat radar bed echoes along hydraulically plausible sinks (Carter and Fricker, 2012).

A large-amplitude ($\sim$600 nT), long-wavelength, positive magnetic anomaly $\sim$ 40-80 km in diameter indicate that both the caldera and central edifice are part of a larger volcanic construct (Blankenship et al. (1993), 3.5). The large magnetic anomaly is associated with a broad uplift of the subglacial crust. The modeled underlying intrusive appears to be several kilometers thick, assuming the material producing the magnetic anomaly has a magnetic susceptibility 0.10 SI (Behrendt et al., 1995). A 10-mGal free-air gravity anomaly is centered over Mt. CASERTZ edifice (Blankenship et al., 1993).

### 3.3.1.2 Kamb Ice Stream subglacial volcano

The joint interpretation of potential fields and radar sounding data collected by the University of Texas Institute for Geophysics (UTIG) identified a subglacial active volcano candidate in the onset region of the Kamb Ice Stream (KIS) of West Antarctica, few tens of km north of the transition zone between the EWM microplate and Ross Subglacial Basin. The lower parts of KIS are known to have
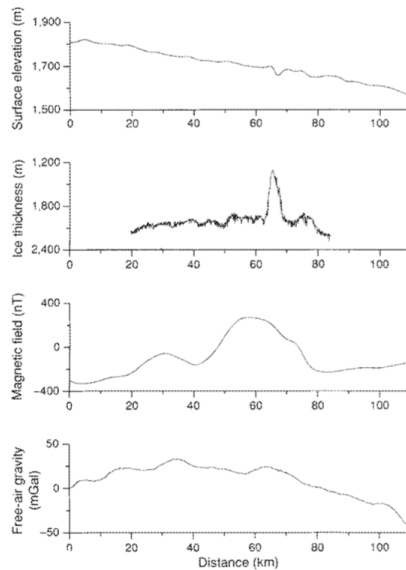
Figure 3.5: Aerogeophysical observations made along one north-south profile of Mt. CASERTZ (from Blankenship et al. (1993)). Surface elevation from laser-altimeter measurements (accurate to 1 m). The anomalous depression in the ice surface is located at 67 km. Ice thickness from SOAR incoherent radar observations. The peak of the central edifice is at 66 km and the rim of the proposed caldera intersects the profile at 53 and 76 km. The magnetic field is shown after removing the geomagnetic reference field and is corrected for ionospheric variations using observations from a fixed base station; the large anomaly between 40 and 80 km is strongly correlated with the volcanic construct which includes the caldera and central edifice. Free-air gravity profile shows a weak 10 mGal anomaly.

been stagnant for the last ~150 years (Retzlaff and Bentley, 1993), while upper ice continues to flow (Price and Newman, 2001).

KIS subglacial volcano was first surveyed in 1992 during the CASERTZ aerogeophysical survey with incoherent radar (see Fig. 3.3 before being partially reflown with HiCARS as part of the ATRS program (Peters et al., 2005a, 2007b). HiCARS focused data shows englacial layers that down dip over the edge of a broad

conical high in the center of the ice stream. Radar sounding over KIS onset region shows a bright sub-ice reflection (Peters et al., 2007b) and high specularity content suggesting the presence of significant water beneath the ice stream (Young et al., 2015).

The joint inversion of the high gravity signal and relatively weak magnetic signature suggests the presence of a subglacial volcano in the area (Filina et al., 2006). This volcanic feature produces a sharp distinctive peak in gravity due to a high density contrast of a magma body in the subsurface with surrounding rocks, but a low magnetic signature only due to a thin layer of extrusive material just beneath the ice.

### 3.3.1.3   Subglacial Lake Whillans

Extraordinary high geothermal flux (285 $\pm$80 mW m$^{-2}$) was measured at Subglacial Lake Whillans (SLW) drilling site as part of the Whillans Ice Stream Subglacial Access Research Drilling (WISSARD) project Fisher et al. (2015). The measurement represents the first direct assessment of geothermal flux into the base of WAIS, obtained with a probe that went $\sim$ 1 m deep into basal sediments. The value of geothermal flux determined at SLW is significantly higher than continental average but representative of areas of active hydrothermal and volcanic activity (e.g. http://www.heatflow.org).

The highly dynamic hydrologic activity observed at the SLW drilling site (Fricker and Padman, 2012) is consistent with fluctuations of basal melt water supply generated by elevated geothermal flux. The site location near the convergence

between Siple Coast's Whillans and Mercer Ice Streams makes changes in the local hydrologic configuration particularly relevant to ice sheet dynamics.

### 3.3.2   WAIS divide sector

The WAIS divide is a region of thick ice and slow to negligible ice flow. Similarly to a continental hydrographic divide, this region separates WAIS into two catchments: one where the ice flows to the Ross Sea, and one where the ice flows to the Amunsden and Weddell Seas. Subglacial volcanic activity in this sector can impact ice flow organization within those catchments, which can ultimately lead to ice divide migration.

WAIS divide is located within the low laying cradle-shaped topography of central WARS, up to 2000 m below sea level, characterized by thin crust (Fretwell et al., 2013; Chaput et al., 2014). It is bounded by EWM crustal block to the South and eMBL to the North.

#### 3.3.2.1   WAIS ice core site

The high precision measurements made in the 3405-m deep borehole at WAIS Divide ice core site (WAIS Divide Project Members, 2013)) represent the first direct measurement of anomalously high subglacial geothermal flux in Antarctica, performed at 50 m above the estimated bedrock depth, where drilling stopped to prevent contamination of the basal hydrology. Site selection for the WAIS Divide ice core had been part of an effort by the ice coring community to find an ice record extending to the last interglacial in West Antarctica. Criteria for site selec-

tion included finding a region with thick ice and slow ice flow, to assure recovery of deep/old and undisturbed/organized ice record. However, despite the great ice thickness ( $> 3000$ m) at the slow ice flow site at the WAIS divide, the ice near the bed proved to be relatively young ( $\sim 68$ ka) compared to shallower cores drilled in central East Antarctica, which was interpreted as the result of high accumulation rates (22 cm a$^1$ at present and $\sim 10$ cm a$^1$ during the Last Glacial Maximum) and basal melt (Buizert et al., 2015).

Interpretation of the temperature measurements in the borehole indicates the ice sheet is melted at the bed at this location and that the basal melting rate is remarkably high, $\sim 1.5$ cm a$^{-1}$. The inferred geothermal heat flux, using thermal data from the ice sheet and a one-dimensional model of ice dynamics, is estimated to be about 140 to 220 mW m$^{-2}$, 4–5 times the continental average. Importantly, the absence of a surface depression at the WAIS Divide site indicates that this high heat flow is likely to be the regional value (horizontal scale $\sim 30$ km), rather than simply a local anomaly (Clow et al., 2012).

### 3.3.2.2   Subglacial caldera complex

A series of positive magnetic anomalies between 400-1200 nT surrounding a central magnetic low ( $\sim$ -150 nT) define the rim of a large subglacial caldera about 70 km in diameter located in the deep ice region between MBL and the WAIS Divide ice core site (Fig. 3.1; Behrendt et al. (1998)). The caldera is surrounded by a low magnetic background (-300 to -500 nT), consistent with a shallow Curie isotherm (Behrendt et al., 1998).

With the exception of C, all other anomalies show no explicit correspondence to subglacial bed topography, as assessed with both incoherent CASERTZ radar and focused AGASEA HiCARS radar. This observation suggests that the source of anomaly C likely consists of erosion resistant pillow lavas, characteristic of eruptions under very thick ice (Behrendt et al., 1998) and supports the interpretation that the caldera complex was recently active under the current, thick WAIS.

### 3.3.2.3 Mt. Thiel

Mt. Thiel was first identified from airborne magnetics and interpreted as composed of erosion-resistant volcanic flows by Behrendt et al. (2002). It has a subglacial topographic relief $\sim 1800$ m high and corresponds to a positive (400 nT) magnetic anomaly situated within the low magnetic background and shallow Curie isotherm surrounding the nearby subglacial caldera complex. Mt. Thiel is located about 100 km distant from the WAIS ice core drilling site and is the hypothesized source of a prominent volcanic ash layer detected at WAIS's ice core (Behrendt, 2013; Dunbar et al., 2011).

### 3.3.2.4 Fissure system

Magnetic anomalies L and M identified by Behrendt et al. (1995) have been analyzed by Danque (2008) using focused HiCARS radar and magnetics from the AGASEA survey. Danque (2008) inferred anomaly L is a warmer, more active feature than anomaly M. In addition, Danque (2008) interpreted an additional anomaly, named H, which corresponds to a significant down draw of layers.

In radargrams, anomaly L shows as a broad, dome-shaped subglacial edifice about 250-300 meter high with a a stair-step morphology and steep ridges on its summit. Coherent radar sounding data over L show eight bright basal reflections (200-500 m in diameter) located along the breaks in the slope between the surrounding plains and the dome of feature L. These bright spots appear in radar profiles as smooth, bright, and specular reflectors located in hydraulic flat regions on the flanks and on the summit of edifice L and are interpreted as subglacial lakes. Two of the potential lakes found on the summit of L are located respectively in a depression on the southeast side of the summit and between the summit ridges. The steep-sided ridges on L could either indicate a recent eruption products or an old ridge that are well preserved by the slow flowing ice near the divide.

Even though the ice surface does not dip over edifice L, the englacial layers have some drawdown over one of these possible lakes, while over the summit of L layers faint out entirely. This might indicate a physical or thermal disturbance over the summit of L that leads to steep layer slopes dipping $>10$ degrees, which is the imaging capabilities of the current 2D-focused SAR processing. A magnetic anomaly $\sim 300$ nT in amplitude is associated to L. The model of the magnetic anomaly is consistent with a large cooling intrusive body hot enough to maintain the subglacial lakes apparent in coherent radar profiles. Because of the position of the lakes with respect to the regional hydraulic potential, it is likely that the lakes are sustained by local sources and not by subglacial water flow.

Anomaly M (Behrendt et al., 1995; Danque, 2008) appears in radargrams as a mound situated along an elongated subglacial ridge oriented nearly east-west,

adjacent to L. Site M is associated with a 300 nT magnetic anomaly, has no corresponding ice surface depression or internal layers drawdowns, and lacks evidence for nearby subglacial lakes. The low topography and smooth sides are consistent with the interpretation that M is the eroded root of a subglacial volcanic edifice (Behrendt et al., 1995), likely older and colder than site L.

Feature H (Danque, 2008) is a large layer drawdown anomaly in the radar englacial layers of the ice sheet located along an area of flat topography adjacent to edifice L. The layer drawdown is identified by a 300 m dip in the deepest visible englacial layers that can be traced for 28 km in length. A small, $\sim$70 m high and $\sim$2 km across topographic relief underlies the layer drawdown for the entire length of the anomaly. Bright, flat, and specular echoes on either side of the bed topography relief indicate subglacial lakes 0.5 km and 1 km in apparent cross-sectional diameter. The layer drawdown is associated with an ice surface depression visible in MOA surface imagery and a $<$ 50 nT magnetic anomaly.

### 3.3.3  Marie Byrd Land sector

Seismic tomography from the broadband seismic Antarctic Polar Earth Observing Network shows evidence for a large thermal anomaly under MBL consistent with a focused hot spot centered beneath the Executive Committee Range (Hansen et al., 2014; Accardo et al., 2014; An et al., 2015; Emry et al., 2015; Lloyd et al., 2015; Heeszel et al., 2016).

### 3.3.3.1 Executive Committee Range

Underground magmatic activity has been identified at the southern tip of the Executive Committee Range (ECR) volcanic chain from passive seismic observations as part of the POLENET/ANET project (Lough et al., 2013). A cluster of DLP seismic episodes was detected in January-February 2010 and March 2011 beneath a subglacial edifice located where present volcanic activity would be expected along the ECR northsouth-migrating volcanic trend.

The active subglacial volcano interpreted by Lough et al. (2013) was directly imaged as part of the Geophysical Investigation of Marie Byrd Land Lithospheric Evolution (GIMBLE) airborne geophysical program and corresponds to a subglacial topographic high $\sim 1000$ m above the surrounding and a 400 nT magnetic anomaly (Lough et al., 2013). GIMBLE also detected significant subglacial water directly downstream of the ECR (Young et al., 2015).

While significant englacial ash layer is imaged in this region, both the observation of tephra bands in a zone of ablating blue ice and the distribution of the ash layer in a wind-oriented streak south of the active subarial Mount Waesche suggest the source is most probably Mount Waesche. Perhaps the strongest argument for a Mount Waesche source is the implausibility of an eruption from the DLP source venting ash to the surface.

### 3.3.4 Amundsen Sea Embayment Sector

The Amundsen Sea Embayment (ASE) is located within the deepest region of WARS. It is bounded by thicker and higher elevation crustal blocks to the

North, South, and South West (EWM, eMBL, and TI respectively), and by the Siple Coast to the West. Within ASE's low and landward sloping bed flow some among the fastest-flowing, most rapidly changing ice streams on Earth currently at risk of rapid collapse (Mouginot et al., 2014), which makes this sector of WAIS a main component in scenarios of rapid deglaciation.

In this sector of WAIS, geothermal flux can have a large impact on ice flow organization and ice streams basal sliding velocity through the production of subglacial melt water. Not only does geothermal flux play a key role on ice flow velocity; importantly, it can also potentially control ice flow initiation along ice divides.

### 3.3.4.1 Hudson Mountains subglacial volcano

Subglacial volcanic activity near the Hudson Mountains was identified by Corr and Vaughan (2008) as the source of a bright, local englacial layer as imaged in radar data. The strong radar reflection covers an elliptical area of about 23,000 km$^2$. The source region for the tephra layer, which has not been overflown with airborne geophysical surveys, was identified using the layer's radar echo strength as a proxy for the tephra thickness and proximity to the volcanic center, and coincides with a subglacial topographic high along the Hudson Mountains characterized by a complex pattern of positive magnetic anomalies (Golynsky et al., 2018). The layer depth dates the eruption at 207 BC +/- 240 years, which matches strong and previously unattributed conductivity signals measured in two nearby ice cores, Byrd Station and Siple Dome (Corr and Vaughan, 2008; Hammer et al., 1997; Kurbatov et al., 2006). Rowley et al. (1986) report anecdotal evidence of recent volcanic ac-

tivity including a report of the "possible presence of steam" in 1974, and a possible eruption seen in satellite data in 1985.

### 3.3.4.2 Thwaites Glacier hot spots

Indirect evidence of elevated geothermal flux from airborne radar sounding data and a subglacial hydrologic model points to spots of localized geothermal flux $\sim 200$ mW/m$^2$ within the Thwaites Glacier catchment (Schroeder et al., 2014a). High geothermal flux is estimated along the ice covered flanks of subaerial volcanoes Mt. Takahe and Mt. Frakes, over subglacial volcano Mt. Thiel, and in correspondence of two circular positive magnetic anomalies associated to subglacial edifices. The spatial distribution of these hot spots at the inception of tributaries and fast flowing ice streams is additional evidence of the potential impact of active volcanism on ice organization and ice sheet dynamics.

## 3.4 Discussion

Active subglacial volcanism in West Antarctica is mostly observed along regions of thinned crust, such as transition margins between crustal blocks and within central WARS (Fig. 3.7). This interpretation is sported by recently published magnetic data (ADMAP2, Golynsky et al. (2018)) which indicates the presence of an additional crustal boundary along the ECR line of volcanoes in MBL.

Within central WARS, active subglacial volcanism is observed within Thwaites Glacier catchment, the Siple Coast, where hot spots have been observed both along the ice covered flanks of two recently active subaereal volcanoes, Mt. Takahe and

Mt. Frakes, and upstream of fast flowing and highly dynamic ice streams; and along the WAIS ice drainage divide region.

The largest gaps in spatial distribution occur within previously defined crustal blocks and the Siple Coast portions of WARS. Observational biases are inevitably introduced by limited data coverage and resolution, which can impair detection criteria and limit the number of active sites identified in any given sector. Moreover, large surveyed portions of West Antarctica have simply not yet been investigated and await systematic investigations of the current status of active subglacial volcanism therein.
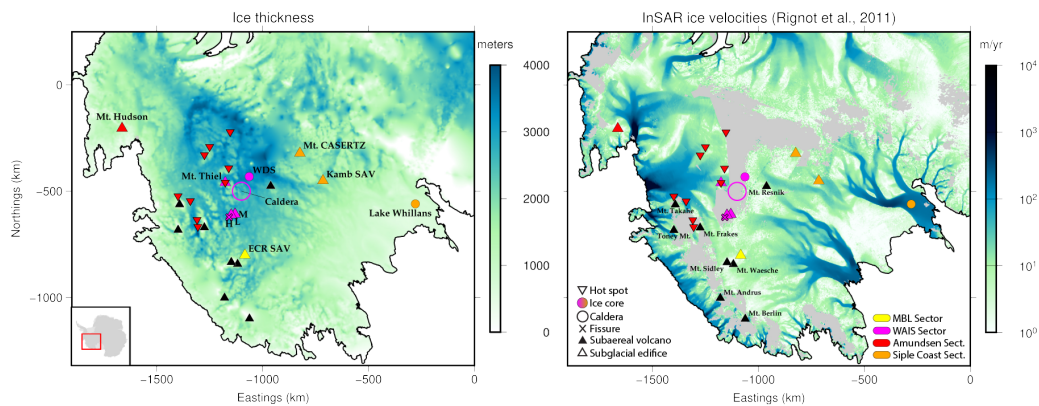


Figure 3.6: Distribution of volcanic edifices over (left) Bedmap2 ice thickness (Fretwell et al., 2013); (right) ice surface velocity (Rignot et al., 2014)

However, other geological and glaciological considerations can explain the spatial distribution of active subglacial sites observed in West Antarctica. Factors such as crustal age and thickness can explain the lack of active subglacial volcanism within sectors characterized by thicker crust such as crustal blocks and the Siple Coast (Chaput et al., 2014). On the other hand, the region of Thwaites Glacier's

main trunk is likely to have cooled, and volcanic activity in the area ceased, since the last emplacement of basaltic wedges during the early mid-Mesozoic stages of WARS formation (Quartini et al., in prep.; Gohl et al., 2013).

Finally, the glaciological regimes in each sector impose biases to the preservation of subglacial volcanic records which can potentially prevent detection of volcanic activity even where present. Subglacial eruptions under thin ice produce more brittle and less consolidated deposits, such as hyaloclastites, compared to eruptions under the high pressure conditions of thicker ice columns, where more erosion-resistant pillow lava flows form. As a result, the products of volcanic activity under thinner ice columns are more prone to erosion and removal by the ice sheet (Behrendt et al., 1998). This is particularly relevant in regions of fast ice flow, such as the Siple Coast and main trunk of Thwaites Glacier (Rignot et al., 2014). While Thwaites Glacier is a region of high driving stresses and thick ice, the Siple Coast ice streams are characterized by thin ice, making this a region particularly prone to loss of subglacial volcanic records.

## 3.5   Conclusions

Active subglacial volcanism is identified throughout West Antarctica, within different geological and glaciological local contexts. The majority of active subglacial volcanic sites in West Antarctica concentrate along crustal boundaries and within central WARS, which are regions of thinned, rifted crust that have been tectonically reactivated during multiple stages of WARS formation (Dalziel, 1992; Quartini et al., in prep.). Subglacial Volcanic sites also overlap with areas of rela-

Table 3.2: List of active subglacial volcanoes in West Antarctica

| Feature | Coordinates | Ice thickness[10] | Bed elevation (Rebounded)[11] | Crustal thickness[12] | Ice flow velocity[13] |
|---|---|---|---|---|---|
| Mt. CASERTZ[1] | 81.88°S, 111.30°W | 1791 m | -79 m (518 m) | 27.5 km | 10 m yr$^{-1}$ |
| KIS Subglacial Volcano[2] | 82.00°S, 113.00°W | 1816 m | -295 m (310 m) | 26.5 km | 14 m yr$^{-1}$ |
| Subglacial Lake Whillans[3] | 84.25°S, 153.50°W | 799 m | -667 m (-400 m) | 25.6 km | 350 m yr$^{-1}$ |
| WAIS ice core Site[4] | 79.47°S, 112.09°W | 3441 m | -1645 m (-498 m) | 22.4 km | 12 m yr$^{-1}$ |
| L edifice[5] | 78.08°S, 117.96°W | 2537 m | -772 m (73 m) | 23.0 km | 16 m yr$^{-1}$ |
| M edifice[5] | 78.23°S, 118.31°W | 2772 m | -1010 m (-86 m) | 23.0 km | 8 m yr$^{-1}$ |
| H anomaly[5] | 77.95°S, 118.24°W | 2923 m | -1158 m (-183 m) | 23.1 km | 5 m yr$^{-1}$ |
| Subglacial Caldera[6] | 78.67°S, 114.50°W | 2820 m | -1012 m (-72 m) | 22.5 km | 8 m yr$^{-1}$ |
| Mt. Thiel[7] | 78.42°S, 111.33°W | 1425 m | 174 m (649 m) | 22.0 km | 7 m yr$^{-1}$ |
| ECR Subglacial Volcano[8] | 77.65°S, 126.77°W | 726 m | 2060 m(2303 m) | 27.6 km | 3 m yr$^{-1}$ |
| Hudson Mts Subglacial Volcano[9] | 74.67°S, 97.00°W | 775 m | 212 m (470 m) | 23.1 km | 2 m yr$^{-1}$ |
| Thwaites hot spots[10] | 78.23°S, 103.12°W | 2220 m | -611 m (128 m) | 22.6 km | 19 m yr$^{-1}$ |
| | 77.93°S, 104.52°W | 1986 m | -533 m (129 m) | 22.2 km | 15 m yr$^{-1}$ |
| | 78.77°S, 108.69°W | 2333 m | -598 m (180 m) | 22.3 km | 2 m yr$^{-1}$ |
| | 78.42°S, 111.33°W | 1424 m | 175 m (649 m) | 22.1 km | 8 m yr$^{-1}$ |
| | 76.67°S, 115.86°W | 3050 m | -1580 m (-563 m) | 23.2km | - * |
| | 76.57°S, 117.08°W | 3068 m | -1525 m (-503 m) | 23.5 km | - * |
| | 79.22°S, 100.89°W | 3000 m | -1041 m (-42 m) | 23.6 km | - * |
| | 76.32°S, 110.51°W | 2139 m | -1021 m (-306 m) | 23.0 km | 168 m yr$^{-1}$ |
| | 76.73°S, 112.16°W | 2671 m | -1388 m (-497 m) | 22.7 km | 108 m yr$^{-1}$ |
| | 76.60°S, 123.08°W | 2808 m | -595 m (340 m) | 24.6 km | 11 m yr$^{-1}$ |

[1] Blankenship et al. (1993); [2]Filina et al. (2008); [3]Fisher et al. (2015); [4]Clow et al. (2012); [5]Danque (2008); [6]Behrendt et al. (1998); [7]Behrendt (2013); [8]Lough et al. (2013); [9]Corr and Vaughan (2008); [10]Schroeder et al. (2014a); [11]Fretwell et al. (2013); [12] Airy isostatic rebound; [13]Chaput et al. (2014); [14]Rignot et al. (2014); * No data.

tively thick ice and slow ice surface flow, both of which are critical conditions for the preservation of volcanic records (Behrendt et al., 1998). By altering the ice's thermal structure and generating basal melt water, heterogeneous geothermal flux has the potential to affect ice dynamics in all sectors of West Antarctica where active subglacial volcanism is observed. Though large areas of both West and East Antarctica have been surveyed but not yet searched for evidence of active subglacial volcanism.
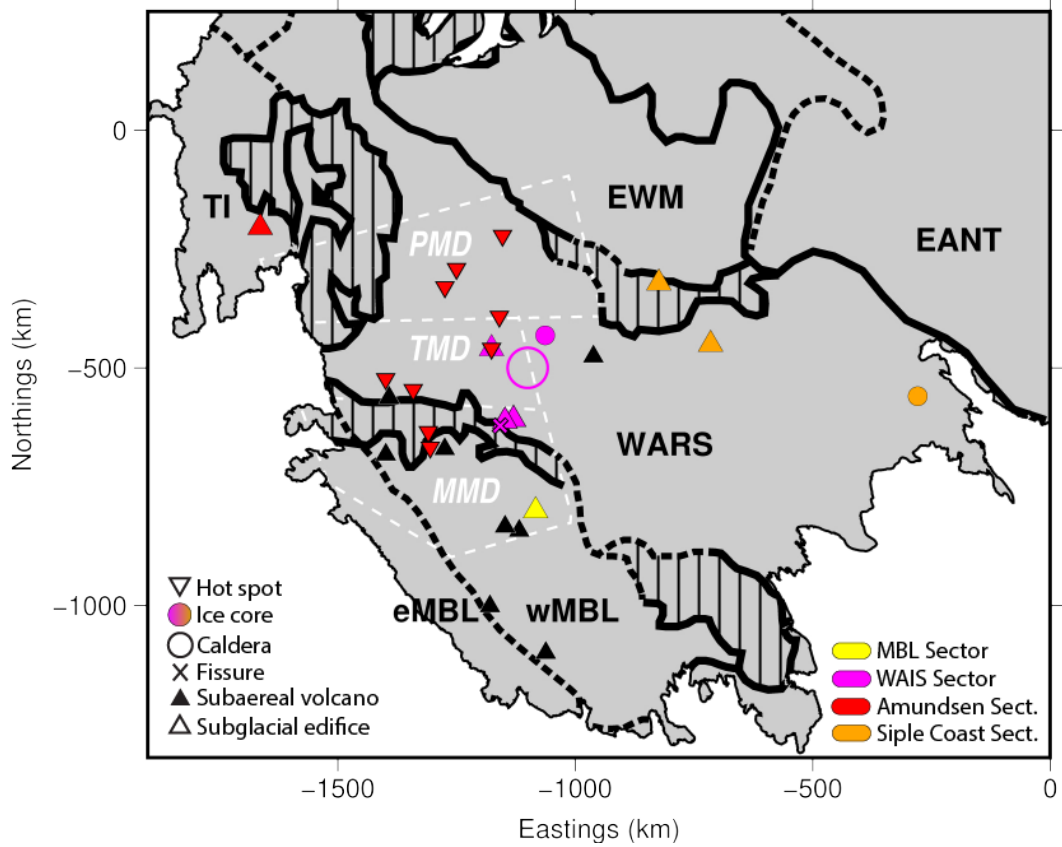
Figure 3.7: Distribution of volcanic edifices over crustal boundaries identified by Diehl et al. (2008) and Quartini et al. (in prep.).

# Chapter 4

# Evidence for elevated subglacial geothermal flux at Marie Byrd Land, Antarctica

## 4.1 Introduction

Marie Byrd Land (MBL) is an area of active volcanism and elevated topography bordering the West Antarctic rift system (WARS), a Jurassic through Cenozoic area of continental extension mostly below sea level. The landward-sloping topography of WARS makes the West Antarctic Ice Sheet (WAIS) that lies within it susceptible to marine instability (Weertman, 1974) and potential collapse in a positive feedback process that may already be under way (Joughin et al., 2014; Rignot et al., 2014).

A potential threats to WAIS stability is posed by elevated geothermal flux, currently one of the least constrained boundary conditions used in ice sheet models. Subglacial volcanic activity and elevated geothermal can contribute to WAIS potential instability by altering providing melt water to the surrounding lowlands, lubricating the base of the ice sheet, and affecting ice flow.

Evidence for active subglacial volcanism and high geothermal flux has been documented throughout the WARS. Anomalously high geothermal flux ($\sim 114 \, mW/m^2$ on average) has been estimated in the Thwaites Glacier catchment using airborne

radar based techniques (Schroeder et al., 2014a), which is consistent with direct point measurements at WAIS Divide ($\sim$240 $mW/m^2$, Clow et al. (2012)) and Subglacial Lake Whillans ($\sim$285$\pm$80 $mW/m^2$, Fisher et al. (2015)) drilling sites.

Receiver function model results have also revealed thinned crust (Chaput et al., 2014) and a significant mantle velocity anomaly beneath volcano Mount Sidney, in the Executive Committee Range (ECR) in MBL (Lloyd et al., 2015). Subglacial volcanic activity had been previously documented along ECR, where a swarm of deep long-period (DLP) earthquakes was registered in 2010 and 2011 by the POLENET seismic network (Lough et al., 2013). DLP, which occur beneath active volcanoes due to deep magmatic activity (Nichols et al., 2011; Okubo and Wolfe, 2008; Power et al., 2004), provided strong evidence of ongoing volcanic activity along the southward end of the ECR, consistent with the north-south progression of activity in the Range recorded between the Miocene and Holocene epochs.

The DLP swarm was sourced $\sim$25 km below a subglacial topographic and magnetic high, as shown by an airborne profile collected during the first season of the Geophysical Investigation of Marie Byrd Land (GIMBLE) project, located $\sim$ 5 $km$ to the east of the swarm center, and by aeromagnetic data from the earlier Airborne Geophysical Survey of Amundsen Embayment project (AGASEA). MBL was further surveyed as part of the second season of GIMBLE (2014-2015), during which airborne profiles were flown directly above the DLP swarm center to collect airborne data over the hypothesized subglacial volcanic edifice.

Seroussi et al. (2017) explored using a version of the ISSM ice sheet model

with a basal melting criteron to investigate the affect of varying the distribution of in geothermal heat flow, consistent with a hotspot in the region of the DLP swarm region (see Figure 4.1). Seroussi et al. (2017) concluded there is no evidence of excess geothermal flux in the region based on the lack of active subglacial lakes (characterized by drainage events that cause changes in ice surface elevation), used in the model as proxy for melt water from which geothermal flux is inferred; however, active lakes are one of two geophysical expressions of subglacial lakes (Young et al., 2015), which can otherwise be detected in radar sounding profiles as hydraulically flat and radar reflective region.

Here we compare the distribution of basal melt detected from radar data (Schroeder et al., 2014a) with predictions of melt water rates produced by high geothermal flux generated by a mantle plume parameterization in ECR (Seroussi et al., 2017). The melt water distribution observed from radar matches that predicted by Seroussi et al. (2017) thus supporting the hypothesis of a hot spot under ECR.

## 4.2  Methods

### 4.2.1  Specularity content

We map the hydrologic configuration of basal melt water by measuring the angular distribution of returned radar energy (Figure 4.2). Water interfaces in pressure equilibrium are highly specular and produce sharp mirror-like reflections, as opposed to diffuse interfaces that scatter energy uniformly in all directions (Schroeder et al., 2016a; Young et al., 2015).

65
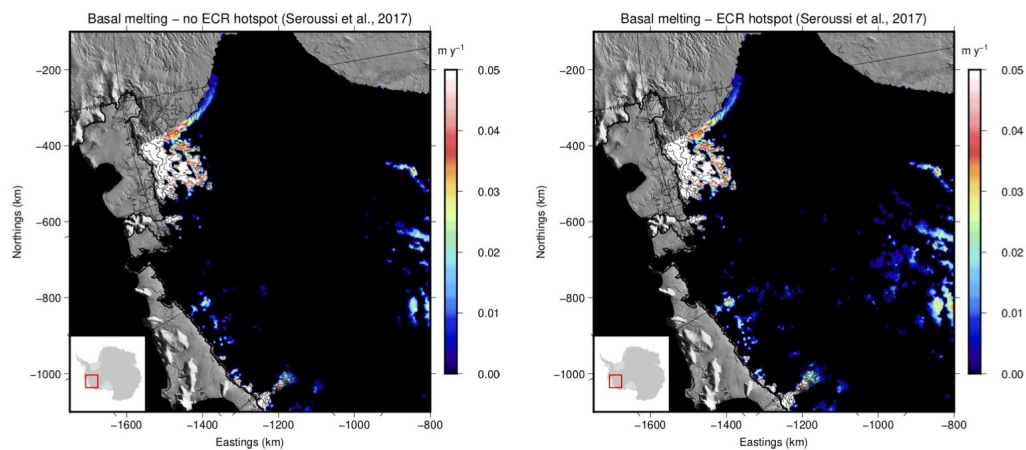
Figure 4.1: Predictions of basal melt (Seroussi et al., 2017) without a hotspot under the ECR (left) and with a hotspot under the ECR DLP site (right), enhanced melting at -1000,-500 is visible on the right plot

Highly specular bed echoes characterize the region upstream of MacAyeal Ice streem, which indicates subglacial water is organized in flat-topped distributed systems such as canals (Schroeder et al., 2013). Additionally, the orthogonal survey configuration makes it possible to evaluate the specularity content of the bed echo along each survey direction independently. The bed echo in this area has an isotropic specularity content, which suggests the subglacial water system itself possesses little variability along the two axes.

### 4.2.2   Bed Reflectivity

The uncertainty in englacial attenuation rates (Gades et al., 2000) for both scattering and reflecting spreading geometries were determined and used to produce maps of the mean and range of observed relative bed echo strengths. We also eval-
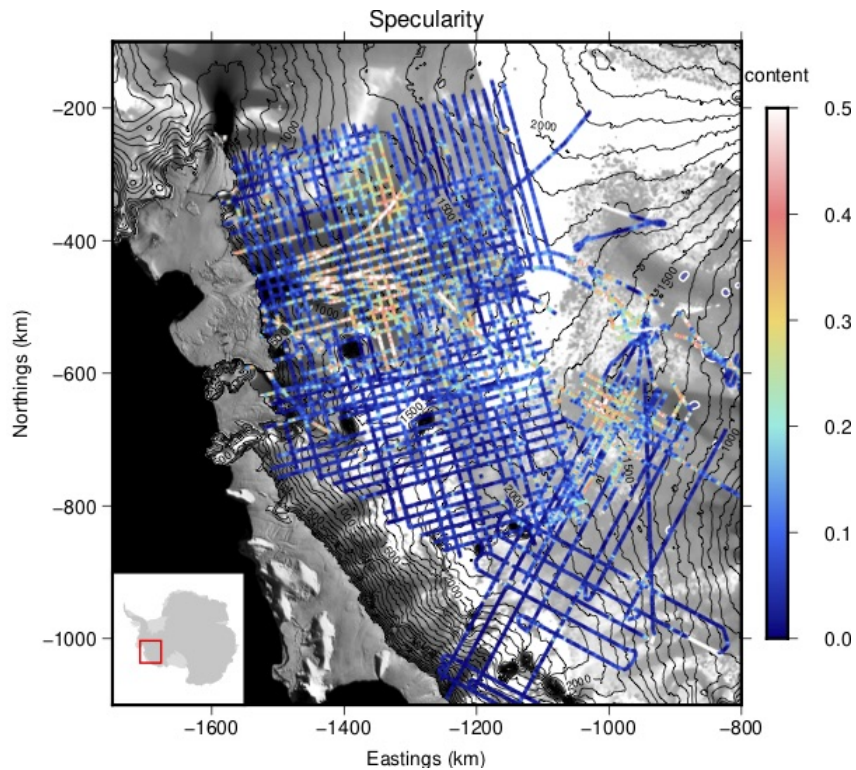
Figure 4.2: Specularity content (from Young et al. (2015), showing region of high specularity at -1000, -550.

uate the variation in englacial attenuation by expanding the coverage of Schroeder et al. (2016b) to the GIMBLE survey (Figure 4.3).

### 4.2.3  Water Routing

Distributed water is in pressure equilibrium with the overlying ice, so its routing is determined by the subglacial hydrologic potential, calculated using our own compilation of radar-derived ice thickness and surface elevation from Bedmap2 (Fretwell et al., 2013). We generated an ensemble of water-routing models by
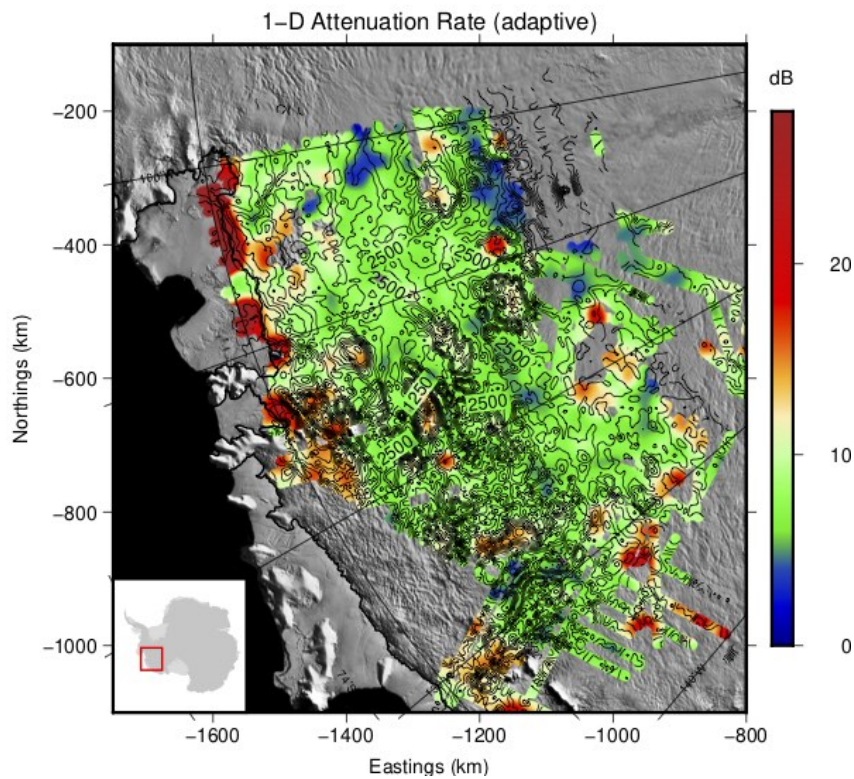
Figure 4.3: Adaptive attenuation rate, one way.

adding noise to the bed topography (at the scale of gridding uncertainties) and selecting those routes that best fit the observed relative bed echo strength distribution (Figure 4.5). The routing models reveal the spatial distribution of melt required to reproduce the pattern of relative echo strength.

## 4.3 Discussion

The extent of the bright layer corresponds to an area of extremely low relative bed echo strength if a constant attenuation rate is used across the region (Figure

68

4.4).

Because our technique ability to estimate geothermal flux relies on accurately detecting the distribution of exceeding basal melt (inverted for from bright bed interfaces), correcting for the appropriate englacial attenuation rates is essential in order to detect the right pattern and amplitude range of bed echo strength. We suggest that the presence of the bright layer might be attenuating the bed echo returns more than what corrected for by our englacial attenuation rate and preventing our technique from detecting melt and therefore geothermal flux in the region.

Our ability to estimate basal melt water distribution relies on accurately correcting for englacial attenuation rates, which impacts the pattern and amplitude range of bed echo strength. We examine the possibility that the presence of the bright layer might be attenuating the bed echo returns more than what corrected for by our englacial attenuation rate and preventing our technique from detecting melt and therefore geothermal flux in the region.

A bright, likely tephra layer (Figure 4.7) covers a vast area within MBL, including the ECR and the potential subglacial volcano identified by (Lough et al., 2013)).

Interestingly, the extent of the bright layer corresponds to the area of extremely low relative bed echo strength (Figure 4.6), when evaluated with a constant ice attenuation rate. Because techniques to estimate geothermal flux rely on accurately detecting the distribution the basal melt (inverted for from bright bed interfaces), correcting for the appropriate englacial attenuation rates is essential in order

to detect the right pattern and amplitude range of bed echoes strength. We suggest that the presence of the bright layer might be attenuating the bed echo returns more than what corrected for by our englacial attenuation rate and preventing our technique from detecting melt and therefore geothermal flux in the region and evaluate that here.

## 4.4   Conclusions

Here we show evidence from radar sounding for distinct hydrologic catchments in the tributary of MacAyeal Ice Stream, directly down flow of the subglacial volcano identified by Lough et al. (2013), that match predictions of basal water melt distribution produced by a mantle plume located beneath the ECR (Seroussi et al., 2017). We also map the distribution of multiple bright englacial layers in MBL and investigate the potential damping effect they pose on basal melt detection and geothermal flux estimates from radar bed echo strength techniques.

We notice that a bright, likely tephra layer (Figure 4.7) covers a vast area within MBL, including the ECR and the potential subglacial volcano identified by Lough et al. (2013) (Figure 4.6). Interestingly, the extent of the bright layer corresponds to an area of extremely low relative bed echo strength (Figure 4.4). Because our technique ability to estimate geothermal flux relies on accurately detecting the distribution of exceeding basal melt (inverted for from bright bed interfaces), correcting for the appropriate englacial attenuation rates is essential in order to detect the right pattern and amplitude range of bed echoes strength. We suggest that the presence of the bright layer might be attenuating the bed echo returns more than

what corrected for by our englacial attenuation rate and preventing our technique from detecting melt and therefore geothermal flux in the region.
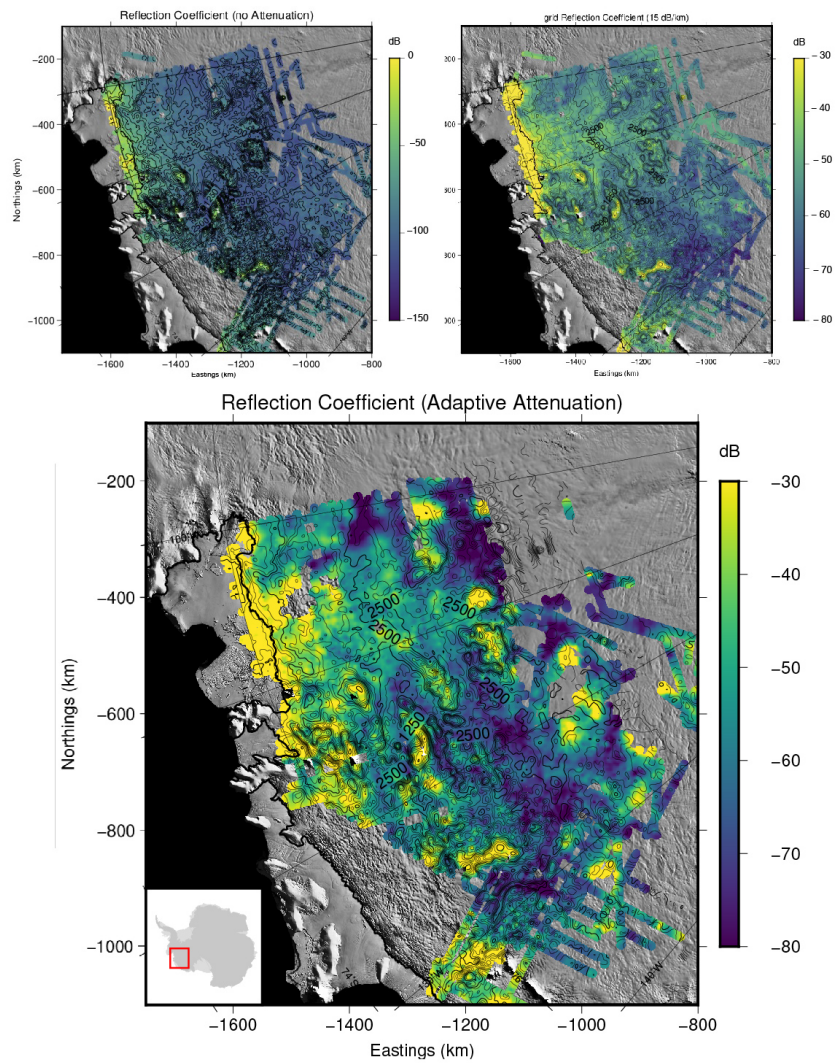
Figure 4.4: Top left: bed echo strength with no attenuation correction; Top right: bed echo strength with constant 15 db/km attenuation correction; Bottom: bed echo strength with adaptive attenuation correction.
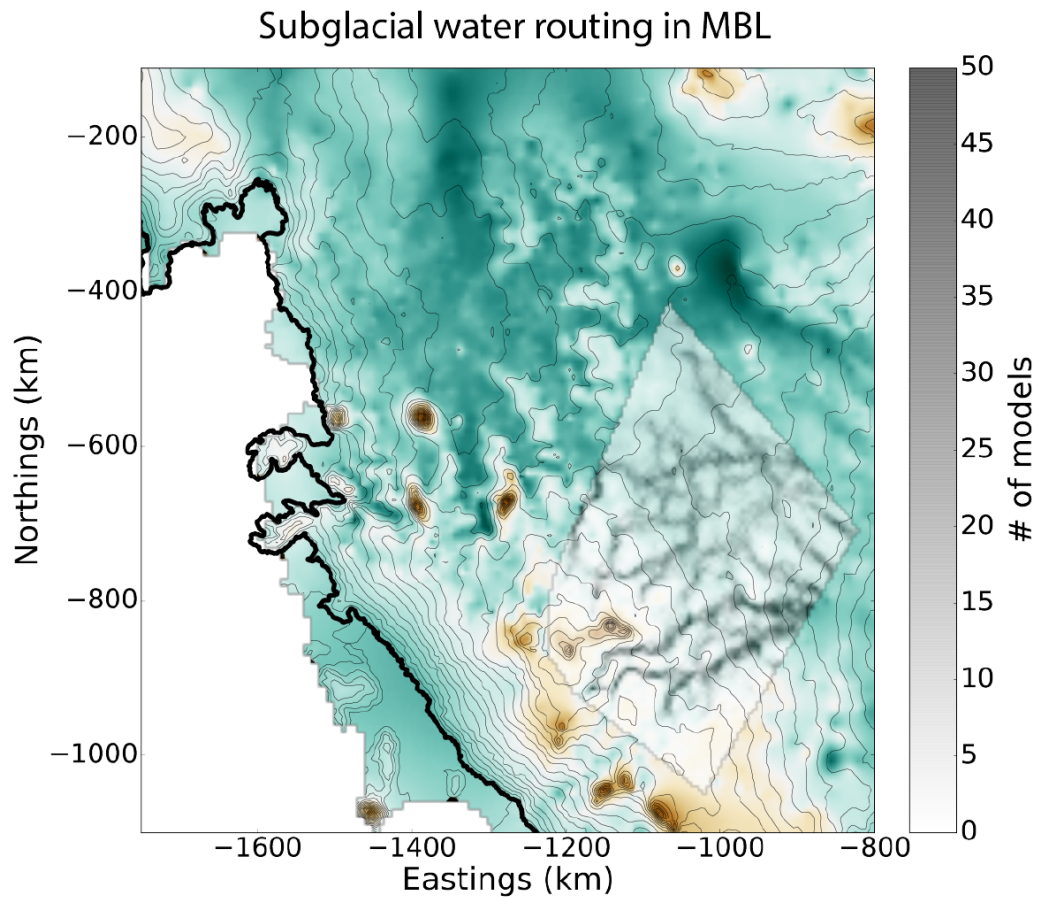
Figure 4.5: Subglacial water routing model. Contour line show hydraulic potential, background color represent bed elevation.
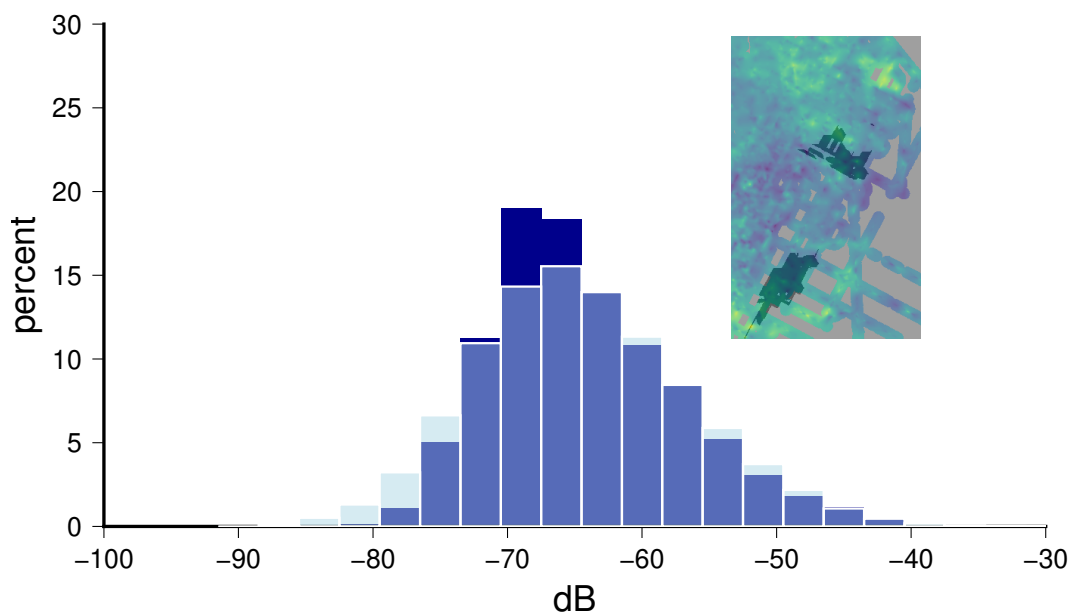
Figure 4.6: Apparent bed reflectivity distribution in areas covered by bright englacial layers (dark blue) and areas with no bright layers (light blue). Ash layer coverage in red over context map.
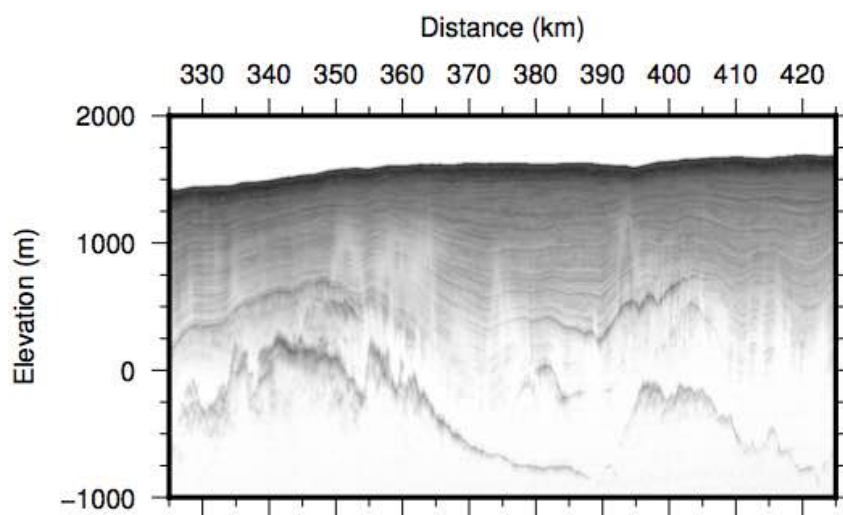


Figure 4.7: Radargram MBL/MKB2l/X21a showing the distribution of ash layers at the location of the detected DLP earthquake cluster by Lough et al. (2013).

# Conclusions

The ice-sheet response to external forcing has major implications for sea level rise, which directly impacts human society and culture. Current sea level rise projections predict nearly a 1 m of sea level rise within the next century at high emission rates (IPCC, 2013); however these predictions do not account for ice sheet collapse. The corresponding loss of land along coast lines world-wide will affect up to 1.4 billion people (Geisler and Currens, 2017), forcing them to relocate to higher elevation regions, and result in significant economic costs due to sea-level rise related effects.

Predictions of sea level rise impact the rate and extent in which both corrective and preventive measures will be implemented to minimize the overall cost of human and economic resources. The accuracy of current predictions has therefore critical immediate implications. This thesis indirectly explores ways in which predictions would benefit from a better understanding of both present ice sheets dynamics and future potential triggers of instability.

Different criteria can be used to identify sectors with distinct geological and glaciological characteristics within West Antarctica and highlight aspects of ice sheet instability over different timescales. From a glaciological standpoint, different sectors can be categorized based on the ice driving stress and flow speed. Areas characterized by high driving stress and fast flow drain WAIS's interior ice towards

the ocean at the highest rates. Therefore, a glaciological classification of sectors aims at localizing regions with the highest potential for ice sheet instability and sea level rise contribution in the immediate to present times. On the other hand, characterizing sectors in terms of their geological character emphasizes the contribution of basal boundary conditions to ice dynamics, which affect ice sheet stability over a wider range of time scales. Improving our ability to correctly recognize geological boundary conditions that trigger ice sheet instability can therefore help projections of sea level rise over longer time scales.

Geothermal flux is a critical boundary condition that affects all sectors of West Antarctica, as shown in Chapter 3. High driving stress regions in WA correspond to areas of marine ice sheet such as THW and PI Glacier catchments. Geothermal flux represents a potentially critical boundary condition in these regions where the supply of melt water can trigger the rapid collapse of the already highly unstable portion of the ice sheet.

On the other hand, in regions characterized by low driving stresses and lack of strong topographic bed control, most of the ice flow occurs through the supply of basal melt water which allows sliding at the base. The low driving stress along the Siple Coast allows thinning of the ice streams and reduced basal shearing, both of which act to cool the bed and promote freezing (Christoffersen et al., 2014). These regions can be largely affected by heterogeneous geothermal flux as they rely on the availability of basal melt water to restore ice flow.

Areas of high geothermal flux are associated with high elevation plateaux supported by hot and buoyant lithosphere. It is therefore hard to justify the pres-

ence of high geothermal flux in areas of low bed topography such as the WARS. However, this apparent incongruity is easily explained by the highly heterogeneous distribution of geothermal flux in West Antarctica, which reconciles WAIS' vulnerability to both the marine ice sheet instability in the colder and lower topography regions of THW and PI, and elevated geothermal flux in the hot and high terrains of MBL.

In Chapter 2, I define three geologically distinct districts in West Antarctica based on interpretation of magnetic anomalies. I evaluate each district in the context of the phases of formation of the West Antarctic Rift System and in terms of their potential for elevated geothermal flux in WARS. My interpretation points to the easter Marie Byrd Land mangetic district (MMD) as the most recently tectonically reactivated region of WARS and the one most likely to currently experience high geothermal flux. The other two identified magnetic districts are located towards Pine Island Glacier (PMD) and in the region comprising Thwaites Glacier catchment (TMD). My interpretation correlates magnetic anomalies in PMD with caldera formation during the mostly extensional stress regime imposed by the Bellinghausen plate's complex rotations in the Late Cretaceous. Finally TMD is interpreted as the relatively oldest and coldest district of WARS, formated at the time of New Zealand's rift from the Antarctic plate margin in the Late Cretaceous and showing no sign of more recent tectonic reactivation. The magnetic fabric in MMD shows evidence for multiple stages of tectonic reactivation and magnetic character loss consistent with crustal heating and magmatic underplating in the mid-Cretaceous and the later emplacement of a hotspot in the Miocene.

In Chapter 3 I identify active subglacial volcanism throughout West Antarctica, within different geological and glaciological local contexts. Despite their differences, all sectors of West Antarctica where active subglacial volcanism is observed, are largely affected by heterogeneous geothermal flux and the resulting generation of basal melt water. In regions with low driving stresses and limited basal friction, such as in the Siple Coast, the flux of basal melt water from local or surrounding geothermal heat sources can significantly impacts ice dynamics by enabling fast ice flow or cause ice stagnation when melt water becomes unavailable.

In Chapter 4, I use a water routing model combined to a glaciological model (Seroussi et al., 2017) to quantify geothermal flux in Marie Byrd Land (MBL). I find areas in the upstream area of MacAyeal ice stream, in the Siple Coast and in Coastal Marie Byrd Land with geothermal flux values $> 150\text{-}200$ mW/m$^2$ and speculate that water discharges from elevated geothermal flux could have implications for MacAyeal ice stream dynamics. I also hypothesize that the presence of a bright, likely tephra layer observed throughout MBL prevents the accurate detection of total basal melt water that feeds the water routing model, ultimately causing the lack of high geothermal flux observed at the location of the active subglacial volcano detected by (Lough et al., 2013).

# Bibliography

N. J. Accardo, D. A. Wiens, S. Hernandez, R. C. Aster, A. Nyblade, A. Huerta, S. Anandakrishnan, T. Wilson, D. S. Heeszel, and I. W. D. Dalziel. Upper mantle seismic anisotropy beneath the west antarctic rift system and surrounding region from shear wave splitting analysis. *Geophysical Journal International*, 198(1):414–429, 2014. doi: 10.1093/gji/ggu117. URL `http://gji.oxfordjournals.org/content/198/1/414.abstract`.

R. P. Ackert, Jr., A. E. Putnam, S. Mukhopadhyay, D. Pollard, R. M. DeConto, M. D. Kurz, and H. W. B. Jr. Controls on interior West Antarctic Ice Sheet elevations: inferences from geologic constraints and ice sheet modeling. *Quaternary Science Reviews*, 65(0):26 – 38, 2013. ISSN 0277-3791. doi: 10.1016/j.quascirev.2012.12.017. URL `http://www.sciencedirect.com/science/article/pii/S0277379113000024`.

R. B. Alley and R. Bindschadler. *The West Antarctic Ice Sheet: Behavior and Environment*, volume 77 of *Antarctic Research Series*, chapter The West Antarctic Ice Sheet and sea level change, pages 1–11. American Geophysical Union, 2001.

M. An, D. A. Wiens, Y. Zhao, M. Feng, A. Nyblade, M. Kanao, Y. Li, A. Maggi, and J.-J. Lévêque. Temperature, lithosphere-asthenosphere boundary, and heat flux beneath the antarctic plate inferred from seismic velocities. *Journal of Geophysical Research: Solid Earth*, 120(12):8720–8742, 2015. ISSN 2169-9356. doi:

10.1002/2015JB011917. URL http://dx.doi.org/10.1002/2015JB011917. 2015JB011917.

J. L. Bamber, R. E. M. Riva, B. L. A. Vermeersen, and A. M. LeBrocq. Reassessment of the potential sea-level rise from a collapse of the West Antarctic Ice Sheet. *Science*, 324(5929):901–903, 5 2009. doi: 10.1126/science. 1169335. URL http://www.sciencemag.org/cgi/content/abstract/324/5929/901.

J. C. Behrendt. Crustal and lithospheric structure of the West Antarctic Rift System from geophysical investigations – a review. *Global and Planetary Change*, 23(1-4):25–44, 1999. URL http://www.sciencedirect.com/science/article/B6VF0-3YJYHD9-2/2/c6721bcdc75f9bfb9514c922763cfcd6.

J. C. Behrendt. The aeromagnetic method as a tool to identify cenozoic magmatism in the west antarctic rift system beneath the west antarctic ice sheet—a review; thiel subglacial volcano as possible source of the ash layer in the waiscore. *Tectonophysics*, 585:124–136, 2013.

J. C. Behrendt, W. E. LeMasurier, A. K. Cooper, F. Tessensohn, A. Tréhu, and D. Damaske. Geophysical studies of the West Antarctic Rift System. *Tectonics*, 10(6):1257–1273, 1991. URL http://dx.doi.org/10.1029/91TC00868.

J. C. Behrendt, D. D. Blankenship, C. A. Finn, R. E. Bell, R. E. Sweeney, S. M. Hodge, and J. M. Brozena. CASERTZ aeromagnetic data reveal late Cenozoic flood basalts(?) in the West Antarctic rift system. *Geology*, 22(6):527–

530, 1994. URL `http://geology.geoscienceworld.org/cgi/content/`
`abstract/22/6/527`.

J. C. Behrendt, D. D. Blankenship, D. Damaske, and A. K. Cooper. Glacial removal
of late cenozoic subglacially emplaced volcanic edifices by the west antarctic ice
sheet. *Geology*, 23(12):1111–1114, 1995.

J. C. Behrendt, C. A. Finn, D. Blankenship, and R. E. Bell. Aeromagnetic evidence
for a volcanic caldera(?) complex beneath the divide of the West Antarctic Ice
Sheet. *Geophysical Research Letters*, 25:4385–4388, 1998.

J. C. Behrendt, D. D. Blankenship, D. L. Morse, C. A. Finn, and R. E. Bell. Sub-
glacial volcanic features beneath the West Antarctic Ice Sheet interpreted from
aeromagnetic and radar ice sounding. *Geological Society, London, Special Pub-
lications;*, 202:337–355, 2002. doi: 10.1144/GSL.SP.2002.202.01.17. URL
`http://dx.doi.org/10.1144/GSL.SP.2002.202.01.17`.

J. C. Behrendt, D. D. Blankenship, D. L. Morse, and R. E. Bell. Shallow-
source aeromagnetic anomalies observed over the West Antarctic Ice Sheet
compared with coincident bed topography from radar ice sounding–new ev-
idence for glacial " removal" of subglacially erupted late cenozoic rift-
related volcanic edifices. *Global and Planetary Change*, 42(1-4):177–
193, 2004. URL `http://www.sciencedirect.com/science/article/`
`B6VF0-4CJVFB9-2/2/f63a09513fb407310c01ebb587a5db5a`.

J. C. Behrendt, C. A. Finn, and D. D. Blankenship. Examples of Models Fit to

Magnetic Anomalies Observed Over Subaerial, Submarine, and Subglacial Volcanoes in the West Antarctic Rift System. *AGU Fall Meeting Abstracts*, pages A2+, Dec. 2006.

B. Bhattacharyya and L.-K. Leu. Analysis of magnetic anomalies over yellowstone national park: mapping of curie point isothermal surface for geothermal reconnaissance. *Journal of Geophysical Research*, 80(32):4461–4465, 1975.

H. Björnsson. Subglacial lakes and jökulhlaups in iceland. *Global and Planetary Change*, 35(3-4):255–271, 2003.

D. D. Blankenship, R. E. Bell, S. M. Hodge, J. M. Brozena, and J. C. Behrendt. Aerogeophysical evidence for active volcanism beneath the West Antarctic Ice Sheet. In *NASA. Goddard Space Flight Center, The First Annual West Antarctic Ice Sheet (WAIS) Science Workshop p 27 (SEE N93-31878 12-46)*, page 27, 1993.

D. D. Blankenship, D. Morse, C. A. Finn, R. E. Bell, M. E. Peters, S. D. Kempf, S. M. Hodge, M. Studinger, J. C. Behrendt, and J. M. Brozena. Geological controls on the initiation of rapid basal motion for West Antarctic Ice Streams: A geophysical perspective including new airborne radar sounding and laser altimetry results. In R. B. Alley and R. A. Bindschadler, editors, *The West Antarctic Ice Sheet: Behavior and Environment*, volume 77 of *Antarctic Research Series*, pages 105–121. American Geophysical Union, 2001.

D. D. Blankenship, S. D. Kempf, and D. A. Young. IceBridge Geometrics 823A Cesium Magnetometer L2 Geolocated Magnetic Anomalies. Digital media, NASA

DAAC at the National Snow and Ice Data Center., Boulder, Colorado USA, 2011a. URL `http://nsidc.org/data/imgeo2.html`.

D. D. Blankenship, D. A. Young, and S. D. Kempf. IceBridge HiCARS 1 L2 Geolocated Ice Thickness. Digital media, NASA DAAC at the National Snow and Ice Data Center, Boulder, Colorado USA, 2011b. URL `http://nsidc.org/data/ir1hi2.html`.

J. Bradshaw, R. Pankhurst, S. Weaver, B. Storey, R. Muir, and T. Ireland. *The Antarctic Region: geological evolution and processes*, chapter New Zealand superterranes recognized in Marie Byrd Land and Thurston Island, pages 429–436. Terra Antartica Publications, 1997.

C. Buizert, K. Cuffey, J. Severinghaus, D. Baggenstos, T. Fudge, E. Steig, B. Markle, M. Winstrup, R. Rhodes, E. Brook, et al. The wais divide deep ice core wd2014 chronology-part 1: Methane synchronization (68-31 ka bp) and the gas age-ice age difference. *Climate of the Past*, 11(2):153, 2015.

S. P. Carter and H. A. Fricker. The supply of subglacial meltwater to the grounding line of the Siple Coast, West Antarctica. *Annals of Glaciology*, 53(60):267–280, 2012. doi: 10.3189/2012AoG60A119.

S. P. Carter, D. D. Blankenship, M. E. Peters, D. A.Young, J. W. Holt, and D. L. Morse. Radar-based subglacial lake classification in Antarctica. *Geochemistry, Geophysics, Geosystems*, 8(Q03016), March 2007. doi: 10.1029/2006GC001408. URL `http://dx.doi.org/10.1029/2006GC001408`.

S. P. Carter, D. D. Blankenship, D. A. Young, and J. W. Holt. Using radar-sounding data to identify the distribution and sources of subglacial water: application to Dome C, East Antarctica. *Journal of Glaciology*, 55(194):1025–1040, 2009. doi: 10.3189/002214309790794931. URL http://dx.doi.org/10.3189/002214309790794931.

J. Chaput, R. C. Aster, A. Huerta, X. Sun, A. Lloyd, D. Wiens, A. Nyblade, S. Anandakrishnan, J. P. Winberry, and T. Wilson. The crustal thickness of West Antarctica. *Journal of Geophysical Research*, pages n/a–n/a, 2014. ISSN 2169-9356. doi: 10.1002/2013JB010642. URL http://dx.doi.org/10.1002/2013JB010642.

P. Christoffersen, M. Bougamont, S. P. Carter, H. A. Fricker, and S. Tulaczyk. Significant groundwater contribution to Antarctic ice streams hydrologic budget. *Geophysical Research Letters*, 41(6):2003–2010, 2014. ISSN 1944-8007. doi: 10.1002/2014GL059250. URL http://dx.doi.org/10.1002/2014GL059250.

T. S. Clarke, P. D. Burkholder, S. B. Smithson, and C. R. Bentley. *The Antarctic Region: geological evolution and processes*, chapter Optimum seismic shooting and recording parameters and a preliminary crustal model for the Byrd Subglacial Basin, Antarctica., pages 485–493. Terra Antartica Publications, 1997.

G. Clow, K. Cuffey, and E. Waddington. High heat-flow beneath the central portion of the west antarctic ice sheet. In *AGU Fall Meeting Abstracts*, 2012.

H. F. J. Corr and D. G. Vaughan. A recent volcanic eruption beneath the West Antarctic ice sheet. *Nature Geoscience*, 1:122–125, 2008. doi: 10.1038/ngeo106. URL http://dx.doi.org/10.1038/ngeo106.

M. L. Curtis. Tectonic history of the ellsworth mountains, west antarctica: Reconciling a gondwana enigma. *GSA Bulletin*, 113(7):939, 2001. doi: 10.1130/0016-7606(2001)113⟨0939:THOTEM⟩2.0.CO;2. URL http://dx.doi.org/10.1130/0016-7606(2001)113<0939:THOTEM>2.0.CO;2.

I. W. Dalziel, L. A. Lawver, I. O. Norton, and L. M. Gahagan. The Scotia Arc: Genesis, evolution, global significance. *Annual Review of Earth and Planetary Sciences*, 41(1):767–793, 2013. doi: 10.1146/annurev-earth-050212-124155. URL http://www.annualreviews.org/doi/abs/10.1146/annurev-earth-050212-124155.

I. W. D. Dalziel. Antarctica: a tale of Two Supercontinents? *Annual Review of Earth and Planetary Sciences*, 20:501–526, 1992. doi: 10.1146/annurev.ea.20.050192.002441. URL http://dx.doi.org/10.1146/annurev.ea.20.050192.002441.

I. W. D. Dalziel and D. H. Elliot. West Antarctica: problem child of Gondwanaland. *Tectonics*, 1(1):3–19, February 1982.

I. W. D. Dalziel and L. A. Lawver. The lithospheric setting of the West Antarctic Ice Sheet. In R. B. Alley and R. Bindschadler, editors, *The West Antarctic Ice Sheet: Behavior and Environment*, volume 77 of *Antarctic Research Series*, pages 13–44. American Geophysical Union, 2001.

T. M. Damiani, T. A. Jordan, F. Ferraccioli, D. A. Young, and D. D. Blankenship. Variable crustal thickness beneath thwaites glacier revealed from airborne gravimetry, possible implications for geothermal heat flux in west antarctica. *Earth and Planetary Science Letters*, 407(0):109 – 122, 2014. ISSN 0012-821X. doi: http://dx.doi.org/10.1016/j.epsl.2014.09.023. URL `http://www.sciencedirect.com/science/article/pii/S0012821X14005780`.

H. A. Danque. Subglacial West Antarctic volcanoes defined by aerogeophysical data and the potential for associated hydrothermal systems. Master's thesis, University of Texas at Austin, 2008.

M. v. W. de Vries, R. G. Bingham, and A. S. Hein. A new volcanic province: an inventory of subglacial volcanoes in west antarctica. *Geological Society, London, Special Publications*, 461:SP461–7, 2017.

R. Decesari, D. Wilson, B. Luyendyk, and M. Faulkner. Cretaceous and Tertiary extension throughout the Ross Sea, Antarctica. In A. Cooper and C. Raymond, editors, *Antarctica: A Keystone in a Changing World*, volume 2007-1047 of *Open-File Report*. USGS, 2007. doi: 0.333/of2007-1047.srp098.

T. M. Diehl. *Gravity Analyses for the Crustal Structure and Subglacial Geology of West Antarctica, Particularly Beneath Thwaites Glacier*. PhD thesis, University of Texas at Austin, 2008.

T. M. Diehl, J. W. Holt, D. D. Blankenship, D. A. Young, T. A. Jordan, and F. Ferraccioli. First airborne gravity results over the Thwaites Glacier catchment, West

Antarctica. *Geochemistry, Geophysics, Geosystems*, 8(Q04011), 2008. doi: 10. 1029/2007GC001878. URL `http://dx.doi.org/10.1029/2007GC001878`.

V. DiVenere, D. V. Kent, and I. W. D. Dalziel. Early cretaceous paleomagnetic results from Marie Byrd Land, West Antarctica: Implications for the Weddellia collage of crustal blocks. *Journal of Geophysical Research: Solid Earth*, 100 (B5):8133–8151, 1995. ISSN 2156-2202. doi: 10.1029/95JB00042. URL `http://dx.doi.org/10.1029/95JB00042`.

A. Donnellan and B. P. Luyendyk. Gps evidence for a coherent antarctic plate and for postglacial rebound in marie byrd land. *Global and Planetary Change*, 42(1-4):305–311, 2004. doi: 10.1016/j.gloplacha. 2004.02.006. URL `http://www.sciencedirect.com/science/article/ B6VF0-4CW4V6V-2/2/3f9d62c3f9afa60608b0426ca164c181`.

N. Dunbar, A. Kurbatov, and W. McIntosh. A maturing tephra record in the west antarctic ice sheet. In *AGU Fall Meeting Abstracts*, 2011.

G. Eagles, K. Gohl, and R. D. Larter. High-resolution animated tectonic reconstruction of the south pacific and west antarctic margin. *Geochemistry, Geophysics, Geosystems*, 5(7):n/a–n/a, 2004. ISSN 1525-2027. doi: 10.1029/ 2003GC000657. URL `http://dx.doi.org/10.1029/2003GC000657`.

E. Emry, A. A. Nyblade, J. Julià, S. Anandakrishnan, R. Aster, D. A. Wiens, A. D. Huerta, and T. J. Wilson. The mantle transition zone beneath west antarctica: Seismic evidence for hydration and thermal upwellings. *Geochemistry, Geophysics, Geosystems*, 16(1):40–58, 2015.

H. Engelhardt. Thermal regime and dynamics of the West Antarctic ice sheet. *Annals of Glaciology*, 39(1):85–92, 2004a. doi: 10.3189/172756404781814203. URL http://dx.doi.org/10.3189/172756404781814203.

H. Engelhardt. Ice temperature and high geothermal flux at Siple Dome, West Antarctica, from borehole measurements. *Journal of Glaciology*, 50 (169):251–256, 2004b. doi: doi:10.3189/172756504781830105. URL http://www.ingentaconnect.com/content/igsoc/jog/2004/00000050/00000169/art00010.

H. Engelhardt, N. Humphrey, B. Kamb, and M. Fahnestock. Physical conditions at the base of a fast moving Antarctic ice stream. *Science*, 248(4951):57–59, 1990. doi: 10.1126/science.248.4951.57. URL http://www.sciencemag.org/content/248/4951/57.abstract.

M. Fahnestock, W. Abdalati, I. Joughin, J. Brozena, and P. Gogineni. High Geothermal Heat Flow, Basal Melt, and the Origin of Rapid Ice Flow in Central Greenland. *Science*, 294(5550):2338–2342, 2001. URL http://www.sciencemag.org/cgi/content/abstract/294/5550/2338.

I. Filina, D. Blankenship, L. Roy, M. Sen, T. Richter, and J. Holt. *Antarctica - Contributions to Global Earth Sciences*, chapter Inversion of airborne gravity data acquired over subglacial lakes in East Antarctica, pages 129–134. Springer-Verlag, Berlin Heidelberg New York, 2006.

I. Y. Filina, D. D. Blankenship, M. Thoma, V. V. Lukin, V. N. Masolov, and M. K. Sen. New 3D bathymetry and sediment distribution in Lake Vostok: Implication

for pre-glacial origin and numerical modeling of the internal processes within the lake. *Earth and Planetary Science Letters*, 276(1-2):106–114, 2008. doi: 10. 1016/j.epsl.2008.09.012. URL `http://www.sciencedirect.com/science/article/B6V61-4TR97R8-2/2/1842625eef201c65b6d15b5dd79206fc`.

C. A. Finn and L. A. Morgan. High-resolution aeromagnetic mapping of volcanic terrain, Yellowstone National Park. *Journal of Volcanology and Geothermal Research*, 115:207–231, 2002. doi: 10.1016/S0377-0273(01)00317-1. URL `http://dx.doi.org/10.1016/S0377-0273(01)00317-1`.

A. T. Fisher, K. D. Mankoff, S. M. Tulaczyk, S. W. Tyler, N. Foley, et al. High geothermal heat flux measured below the west antarctic ice sheet. *Science advances*, 1(6):e1500093, 2015.

C. Fox Maule, M. E. Purucker, N. Olsen, and K. Mosegaard. Heat flux anomalies in Antarctica revealed by satellite magnetic data. *Science*, 309:464–467, 2005. ISSN 5733. URL `http://www.sciencemag.org/cgi/content/abstract/309/5733/464`.

P. Fretwell, H. D. Pritchard, D. G. Vaughan, J. L. Bamber, N. E. Barrand, R. Bell, C. Bianchi, R. G. Bingham, D. D. Blankenship, G. Casassa, G. Catania, D. Callens, H. Conway, A. J. Cook, H. F. J. Corr, D. Damaske, V. Damm, F. Ferraccioli, R. Forsberg, S. Fujita, Y. Gim, P. Gogineni, J. A. Griggs, R. C. A. Hindmarsh, P. Holmlund, J. W. Holt, R. W. Jacobel, A. Jenkins, W. Jokat, T. Jordan, E. C. King, J. Kohler, W. Krabill, M. Riger-Kusk, K. A. Langley, G. Leitchenkov, C. Leuschen, B. P. Luyendyk, K. Matsuoka, J. Mouginot, F. O.

Nitsche, Y. Nogi, O. A. Nost, S. V. Popov, E. Rignot, D. M. Rippin, A. Rivera, J. Roberts, N. Ross, M. J. Siegert, A. M. Smith, D. Steinhage, M. Studinger, B. Sun, B. K. Tinto, B. C. Welch, D. Wilson, D. A. Young, C. Xiangbin, and A. Zirizzotti. Bedmap2: improved ice bed, surface and thickness datasets for Antarctica. *The Cryosphere*, 7:375–393, 2013. doi: 10.5194/tc-7-375-2013. URL http://dx.doi.org/10.5194/tc-7-375-2013.

H. A. Fricker and L. Padman. Thirty years of elevation change on Antarctic Peninsula ice shelves from multimission satellite radar altimetry. *Journal of Geophysical Research*, 117(C2):n/a–n/a, 2012. ISSN 2156-2202. doi: 10.1029/2011JC007126. URL http://dx.doi.org/10.1029/2011JC007126.

T. Fudge, G. Clow, H. Conway, K. Cuffey, M. Koutnik, T. Neumann, K. Taylor, and E. Waddington. High basal melt at the WAIS-Divide ice-core site. In *WAIS Workshop 2012*, Eatonville, Washington, U.S.A., 2012.

S. Fujita, H. Maeno, S. Uratsuka, T. Furukawa, S. Mae, Y. Fujii, and O. Watanabe. Nature of radio echo layering in the Antarctic ice sheet detected by a two-frequency experiment. *Journal of Geophysical Research*, 104(B6):13049–13060, 1999. doi: 10.1029/1998JB900034. URL http://dx.doi.org/10.1029/1998JB900034.

A. M. Gades, C. F. Raymond, H. Conway, and R. W. Jacobel. Bed properties of Siple Dome and adjacent ice streams, West Antarctica, inferred from radio-echo sounding measurements. *Journal of Glaciology*, 46(152):88–94, 2000.

doi: 10.3189/172756500781833467. URL http://dx.doi.org/10.3189/172756500781833467.

C. Geisler and B. Currens. Impediments to inland resettlement under conditions of accelerated sea level rise. *Land Use Policy*, 66:322–330, 2017.

J. A. Goff, E. M. Powell, D. A. Young, and D. D. Blankenship. Conditional simulation of Thwaites Glacier bed topography for flow models: Incorporating inhomogeneous statistics and channelized morphology. *Journal of Glaciology*, 60(222): 635–646, 2014. doi: 10.3189/2014JoG13J200. URL http:/dx.doi.org/10.3189/2014JoG13J200.

K. Gohl, F. Nitsche, and H. Miller. Seismic and gravity data reveal tertiary interplate subduction in the bellingshausen sea, southeast pacific. *Geology*, 25(4):371, 1997. doi: 10.1130/0091-7613(1997)025⟨0371:SAGDRT⟩2.3.CO;2. URL http://dx.doi.org/10.1130/0091-7613(1997)025<0371:SAGDRT>2.3.CO;2.

K. Gohl, A. Denk, G. Eagles, and F. Wobbe. Deciphering tectonic phases of the Amundsen Sea Embayment shelf, West Antarctica, from a magnetic anomaly grid. *Tectonophysics*, 585(0):113 – 123, 2013. ISSN 0040-1951. doi: 10.1016/j.tecto.2012.06.036. URL http://www.sciencedirect.com/science/article/pii/S0040195112003617.

A. V. Golynsky, F. Ferraccioli, J. K. Hong, D. A. Golynsky, R. R. B. von Frese, D. A. Young, D. D. Blankenship, J. W. Holt, S. V. Ivanov, A. V. Kiselev, V. N.

Masolov, G. Eagles, K. Gohl, W. Jokat, D. Damaske, C. Finn, A. Aitken, R. E. Bell, E. Armadillo, T. A. Jordan, E. Bozzo, G. Caneva, R. Forsberg, M. Ghidella, J. Galindo-Zaldivar, F. Bohoyo, Y. M. Martos, Y. Nogi, E. Quartini, and H. R. Kim. New magnetic anomaly map of the Antarctic. *Geophysical Research Letters*, 2018.

P. Gudmandsen. Electromagnetic probing of ice. In J. R. Wait, editor, *Electromagnetic Probing in Geophysics*, pages 321–348. Golem Press, Colorado, 1971.

M. T. Gudmundsson. Ice-volcano interaction at the subglacial grímsvötn volcano, iceland. *Glaciers, Ice Sheets and Volcanoes: A Tribute to Mark F. Meier*, page 34, 1996.

M. T. Gudmundsson and T. Högnadóttir. Volcanic systems and calderas in the vatnajökull region, central iceland: Constraints on crustal structure from gravity data. *Journal of Geodynamics*, 43(1):153–169, 2007.

C. U. Hammer, H. B. Clausen, and J. Langway, C. C. 50,000 years of recorded global volcanism. *Climatic Change*, 35(1):1–15, 1997. doi: 10.1023/A: 1005344225434. URL http://dx.doi.org/10.1023/A%3A1005344225434.

S. E. Hansen, J. H. Graw, L. M. Kenyon, A. A. Nyblade, D. A. Wiens, R. C. Aster, A. D. Huerta, S. Anandakrishnan, and T. Wilson. Imaging the Antarctic mantle using adaptively parameterized P-wave tomography: evidence for heterogeneous structure beneath West Antarctica. *Earth and Planetary Science Letters*, 408(0):66 − 78, 2014. ISSN 0012-821X. doi: http://dx.doi.org/10.

1016/j.epsl.2014.09.043. URL `http://www.sciencedirect.com/science/article/pii/S0012821X14006062`.

D. S. Heeszel, D. A. Wiens, S. Anandakrishnan, R. C. Aster, I. W. D. Dalziel, A. D. Huerta, A. A. Nyblade, T. J. Wilson, and J. P. Winberry. Upper mantle structure of central and West Antarctica from array analysis of Rayleigh wave phase velocities. *Journal of Geophysical Research: Solid Earth*, 121(3):1758–1775, 2016. doi: 10.1002/2015JB012616. URL `https://agupubs.onlinelibrary.wiley.com/doi/abs/10.1002/2015JB012616`.

R. C. Hindmarsh, G. J. Leysinger Vieli, M. J. Raymond, and G. H. Gudmundsson. Draping or overriding: the effect of horizontal stress gradients on internal layer architecture in ice sheets. *Journal of geophysical research: earth surface*, 111 (F2), 2006.

M. P. Hochstein and S. Soengkono. Magnetic anomalies associated with high temperature reservoirs in the taupo volcanic zone (new zealand). *Geothermics*, 26 (1):1 – 24, 1997. ISSN 0375-6505. doi: https://doi.org/10.1016/S0375-6505(96)00028-4. URL `http://www.sciencedirect.com/science/article/pii/S0375650596000284`.

J. W. Holt, D. D. Blankenship, D. L. Morse, D. A. Young, M. E. Peters, S. D. Kempf, T. G. Richter, D. G. Vaughan, and H. Corr. New boundary conditions for the West Antarctic ice sheet: Subglacial topography of the Thwaites and Smith Glacier catchments. *Geophysical Research Letters*, 33(L09502), May

2006a. doi: 10.1029/2005GL025561. URL `http://dx.doi.org/10.1029/2005GL025561`.

J. W. Holt, M. E. Peters, S. D. Kempf, D. L. Morse, and D. D. Blankenship. Echo source discrimination in single-pass airborne radar sounding data from the Dry Valleys, Antarctica: Implications for orbital sounding of Mars. *Journal of Geophysical Research*, 111, June 2006b. doi: 10.1029/2005JE002525. URL `http://dx.doi.org/10.1029/2005JE002525`.

IPCC. Summary for policymakers. In T. Stocker, D. Qin, G.-K. Plattner, M. Tignor, S. Allen, J. Boschung, A. Nauels, Y. Xia, V. Bex, and P. Midgley, editors, *Climate Change 2013: The Physical Science Basis. Contribution of Working Group I to the Fifth Assessment Report of the Intergovernmental Panel on Climate Change*, pages 1–29. Cambridge University Press, Cambridge, United Kingdom and New York, NY, USA, 2013.

N. A. Iverson, R. Lieb-Lappen, N. W. Dunbar, R. Obbard, E. Kim, and E. Golden. The first physical evidence of subglacial volcanism under the west antarctic ice sheet. *Scientific reports*, 7(1):11457, 2017.

R. W. Jacobel, A. M. Gades, D. L. Gottschling, S. M. Hodge, and D. L. Wright. Interpretation of radar-detected internal layer folding in West Antarctic ice streams. *Journal of Glaciology*, 39(133):528–537, 1993.

J. S. Johnson, M. J. Bentley, and K. Gohl. First exposure ages from the Amundsen Sea Embayment, West Antarctica: the Late Quaternary context for recent

thinning of Pine Island, Smith, and Pope Glaciers. *Geology*, 36(3):223–226, March 2008. doi: 10.1130/G24207A.1. URL http://dx.doi.org/10.1130/G24207A.1.

I. Joughin, B. E. Smith, and B. Medley. Marine ice sheet collapse potentially under way for the thwaites glacier basin, west antarctica. *Science*, 344(6185):735–738, 2014. doi: 10.1126/science.1249055. URL http://www.sciencemag.org/content/344/6185/735.abstract.

I. R. Joughin, S. M. Tulaczyk, J. L. Bamber, D. D. Blankenship, J. W. Holt, T. A. Scambos, and D. G. Vaughan. Basal conditions for Pine Island and Thwaites Glaciers, West Antarctica, determined using satellite and airborne data. *Journal of Glaciology*, 55(190):245–257, 2009.

B. Kamb. Basal zone of the West Antarctic ice streams and its role in lubrication of their rapid motion. In R. B. Alley and R. A. Bindschadler, editors, *The West Antarctic Ice Sheet: Behavior and Environment*, volume 77 of *Antarctic Research Series*, pages 157–200. American Geophysical Union, 2001.

G. D. Karner, M. Studinger, and R. E. Bell. Gravity anomalies of sedimentary basins and their mechanical implications: Application to the Ross Sea basins, West Antarctica. *Earth and Planetary Science Letters*, 235(3-4): 577–596, 2005. URL http://www.sciencedirect.com/science/article/B6V61-4GBD6VK-1/2/4816aa5e33bbfbb58eb8583a3a8c1e83.

A. V. Kurbatov, G. A. Zielinski, N. W. Dunbar, P. A. Mayewski, E. A. Meyerson, S. B. Sneed, and K. C. Taylor. A 12,000 year record of explosive volcanism in

the Siple Dome Ice Core, West Antarctica. *Journal of Geophysical Research: Atmospheres*, 111(D12), 2006. doi: 10.1029/2005JD006072. URL `https://agupubs.onlinelibrary.wiley.com/doi/abs/10.1029/2005JD006072`.

E. Larour, M. Morlighem, H. Seroussi, J. Schiermeier, and E. Rignot. Ice flow sensitivity to geothermal heat flux of pine island glacier, antarctica. *Journal of Geophysical Research*, 117(F4):n/a–n/a, 2012. ISSN 2156-2202. doi: 10.1029/2012JF002371. URL `http://dx.doi.org/10.1029/2012JF002371`.

R. D. Larter, A. P. Cunningham, P. F. Barker, K. Gohl, and F. O. Nitsche. Tectonic evolution of the pacific margin of antarctica 1. late cretaceous tectonic reconstructions. *Journal of Geophysical Research: Solid Earth*, 107(B12), 2002.

L. A. Lavwer and L. M. Gahagan. Constraints on timing of extension in the Ross Sea region. *Terra Antarctica*, 1(3):545–552, 1994.

W. E. LeMasurier. Marie byrd land. In W. E. LeMasurier, J. W. Thomson, P. E. Baker, P. R. Kyle, P. Rowley, J. L. Smellie, and W. Verwoerd, editors, *Volcanoes of the Antarctic Plate and Southern Oceans*, volume 48 of *Antarctic Research Series*, chapter 3, pages 146–255. American Geophysical Union, 1990. ISBN 9781118664728. doi: 10.1029/AR048p0146. URL `http://dx.doi.org/10.1029/AR048p0146`.

W. E. LeMasurier. Neogene extension and basin deepening in the West Antarctic rift inferred from comparisons with the East African rift and other analogs. *Geology*, 36(3):247–250, March 2008. doi: 10.1130/G24363A.1. URL `http://dx.doi.org/10.1130/G24363A.1`.

W. E. LeMasurier and C. A. Landis. *The Antarctic Region: geological evolution and processes*, chapter The West Antarctic erosion surface: its role in determining the timing of mantle plume activity, uplift, and erosion, during late Cretaceous–Cenozoic, pages 481–484. Terra Antartica Publications, 1997.

W. E. LeMasurier and D. C. Rex. Evolution of linear volcanic ranges in marie byrd land, west antarctica. *Journal of Geophysical Research*, 94(B6):7223–7236, 1989.

A. J. Lloyd, D. A. Wiens, A. A. Nyblade, S. Anandakrishnan, R. C. Aster, A. D. Huerta, T. J. Wilson, I. W. Dalziel, P. J. Shore, and D. Zhao. A seismic transect across West Antarctica: Evidence for mantle thermal anomalies beneath the bentley subglacial trench and the marie byrd land dome. *Journal of Geophysical Research: Solid Earth*, pages n/a–n/a, 2015. ISSN 2169-9356. doi: 10.1002/2015JB012455. URL http://dx.doi.org/10.1002/2015JB012455. 2015JB012455.

A. C. Lough, D. A. Wiens, C. G. Barcheck, S. Anandakrishnan, R. C. Aster, D. D. Blankenship, A. D. Huerta, A. Nyblade, D. A. Young, and T. J. Wilson. Seismic detection of an active subglacial magmatic complex in Marie Byrd Land, Antarctica. *Nature Geoscience*, 6:1031–1035, 2013. doi: 10.1038/ngeo1992.

B. P. Luyendyk, C. C. Sorlien, D. S. Wilson, L. R. Bartek, and C. S. Siddoway. Structural and tectonic evolution of the Ross Sea rift in the Cape Colbeck region, Eastern Ross Sea, Antarctica. *Tectonics*, 20(6):933–958, 2001. URL http://dx.doi.org/10.1029/2000TC001260.

K. Matsuoka. Pitfalls in radar diagnosis of ice-sheet bed conditions: Lessons from englacial attenuation models. *Geophysical Research Letters*, 38(5), 03 2011. doi: 10.1029/2010GL046205. URL http://dx.doi.org/10.1029/2010GL046205.

D. Morse, D. Blankenship, E. Waddington, and T. Neumann. A site for deep ice coring in West Antarctica: Results from aerogeophysical surveys and thermo-kinematic modeling. *Annals of Glaciology*, 35:36–44, 2002.

J. Mouginot, E. Rignot, and B. Scheuchl. Sustained increase in ice discharge from the Amundsen Sea Embayment, West Antarctica, from 1973 to 2013. *Geophysical Research Letters*, 41(5):1576–1584, 2014. ISSN 1944-8007. doi: 10.1002/2013GL059069. URL http://dx.doi.org/10.1002/2013GL059069.

S. B. Mukasa and I. W. D. Dalziel. Marie Byrd Land, West Antarctica: Evolution of Gondwana's Pacific margin constrained by zircon U-Pb geochronology and feldspar common-Pb isotopic compositions. *Geological Society of America Bulletin*, 112(4):611–627, 4 2000. URL http://gsabulletin.gsapubs.org/cgi/content/abstract/112/4/611.

N. A. Nereson, C. F. Raymond, E. D. Waddington, and R. W. Jacobel. Recent migration of Siple Dome ice divide, West Antarctica. *Journal of Glaciology*, 44 (148):643–652, 1998.

M. Nichols, S. Malone, S. Moran, W. Thelen, and J. Vidale. Deep long-period earthquakes beneath washington and oregon volcanoes. *Journal of Volcanology and Geothermal Research*, 200(3-4):116–128, 2011.

S. Nowicki, R. A. Bindschadler, A. Abe-Ouchi, A. Aschwanden, E. Bueler, H. Choi, J. Fastook, G. Granzow, R. Greve, G. Gutowski, U. Herzfeld, C. Jackson, J. Johnson, C. Khroulev, E. Larour, A. Levermann, W. H. Lipscomb, M. A. Martin, M. Morlighem, B. R. Parizek, D. Pollard, S. F. Price, D. Ren, E. Rignot, F. Saito, T. Sato, H. Seddik, H. Seroussi, K. Takahashi, R. Walker, and W. L. Wang. Insights into spatial sensitivities of ice mass response to environmental change from the SeaRISE ice sheet modeling project I: Antarctica. *Journal of Geophysical Research: Earth Surface*, 118:1002–1024, 2013. ISSN 2169-9011. doi: 10.1002/jgrf.20081. URL `http://dx.doi.org/10.1002/jgrf.20081`.

P. G. Okubo and C. J. Wolfe. Swarms of similar long-period earthquakes in the mantle beneath mauna loa volcano. *Journal of Volcanology and Geothermal Research*, 178(4):787–794, 2008.

R. J. Pankhurst, S. D. Weaver, J. D. Bradshaw, B. C. Storey, and T. R. Ireland. Geochronology and geochemistry of pre-Jurassic superterranes in Marie Byrd Land, Antarctica. *Journal of Geophysical Research*, 103(B2):2529–2547, 1998. URL `http://www.agu.org/pubs/crossref/1998/97JB02605.shtml`.

L. Peters, S. Anandakrishnan, R. B. Alley, and A. Smith. Extensive storage of basal meltwater in the onset region of a major West Antarctic ice stream. *Geology*, 35 (3):251–254, March 2007a. doi: 10.1130/G23222A.1. URL `http://dx.doi.org/10.1130/G23222A.1`.

M. E. Peters, D. D. Blankenship, and D. L. Morse. Analysis techniques for coherent airborne radar sounding: Application to West Antarctic ice streams. *Journal of*

*Geophysical Research*, 110(B06303), 2005a. doi: 10.1029/2004JB003222. URL `http://dx.doi.org/10.1029/2004JB003222`.

M. E. Peters, D. D. Blankenship, and D. L. Morse. Analysis techniques for coherent airborne radar sounding: Application to West Antarctic ice streams. *Journal of Geophysical Research*, 110(B06303), 2005b. doi: 10.1029/2004JB003222. URL `http://dx.doi.org/10.1029/2004JB003222`.

M. E. Peters, D. D. Blankenship, S. P. Carter, D. A. Young, S. D. Kempf, and J. W. Holt. Along-track focusing of airborne radar sounding data from West Antarctica for improving basal reflection analysis and layer detection. *IEEE Transactions on Geoscience and Remote Sensing*, 45(9):2725–2736, September 2007b. doi: 10. 1109/TGRS.2007.897416. URL `http://dx.doi.org/10.1109/TGRS.2007. 897416`.

M. E. Peters, D. D. Blankenship, D. E. Smith, J. W. Holt, and S. D. Kempf. The distribution and classification of bottom crevasses from radar sounding of a large tabular iceberg. *Geoscience and Remote Sensing Letters, IEEE*, 4(1):142–146, 2007c.

M. Pilkington and J. B. Thurston. Draping corrections for aeromagnetic data: line-versus grid-based approaches. *Exploration Geophysics*, 32:95–101, 2001.

S. Planke and O. Eldholm. Seismic response and construction of seaward dipping wedges of flood basalts: Vøring volcanic margin. *Journal of Geophysical Research: Solid Earth*, 99(B5):9263–9278, 1994.

D. Pollard and R. M. DeConto. Hysteresis in Cenozoic Antarctic ice-sheet variations. *Global and Planetary Change*, 45:9–21, 2005. URL `http://adsabs.harvard.edu/cgi-bin/nph-bib_query?bibcode=2005GPC....45....9P&db_key=PHY`.

D. Pollard and R. M. DeConto. Modelling West Antarctic ice sheet growth and collapse through the past five million years. *Nature*, 458(7236):329–332, 2009. doi: 10.1038/nature07809. URL `http://dx.doi.org/10.1038/nature07809`.

D. Pollard, R. M. DeConto, and R. B. Alley. Potential Antarctic Ice Sheet retreat driven by hydrofracturing and ice cliff failure. *Earth and Planetary Science Letters*, 412(0):112–121, 2 2015. doi: http://dx.doi.org/10.1016/j.epsl.2014.12.035. URL `http://www.sciencedirect.com/science/article/pii/S0012821X14007961`.

J. Power, S. Stihler, R. White, and S. Moran. Observations of deep long-period (dlp) seismic events beneath aleutian arc volcanoes; 1989–2002. *Journal of Volcanology and Geothermal Research*, 138(3-4):243–266, 2004.

C. P. Price and D. E. Newman. Using the r/s statistic to analyze ae data. *Journal of Atmospheric and Solar-Terrestrial Physics*, 63(13):1387–1397, 9 2001. URL `http://www.sciencedirect.com/science/article/B6VHB-43F8MWP-5/2/eeddaf1cec3fc168718b034ca3b08d37`.

E. Quartini, D. A. Young, and D. D. Blankenship. Tectonic and thermal evolution of the west antarctic margin under thwaites glacier from aeromagnetics. *in prep.*, in prep.

C. F. Raymond. Deformation in the vicinity of ice divides. *Journal of Glaciology*, 29(103):357–373, 1983.

R. Retzlaff and C. R. Bentley. Timing of stagnation of Ice Stream C, West Antarctica, from short-pulse radar studies of buried surface crevasses. *Journal of Glaciology*, 39(133):553–561, 1993. doi: 10.3189/S0022143000016440.

E. Rignot, J. Mouginot, and B. Scheuchl. Antarctic grounding line mapping from differential satellite radar interferometry. *Geophys. Res. Lett.*, 38(10), 05 2011a. doi: 10.1029/2011GL047109. URL `http://dx.doi.org/10.1029/2011GL047109`.

E. Rignot, J. Mouginot, M. Morlighem, H. Seroussi, and B. Scheuchl. Widespread, rapid grounding line retreat of Pine Island, Thwaites, Smith, and Kohler glaciers, West Antarctica, from 1992 to 2011. *Geophysical Research Letters*, 41(10): 3502–3509, 2014. ISSN 1944-8007. doi: 10.1002/2014GL060140. URL `http://dx.doi.org/10.1002/2014GL060140`.

E. J. Rignot, J. Mouginot, and B. Scheuchl. Ice flow of the Antarctic ice sheet. *Science*, 333(6048):1427–1430, 2011b. doi: 10.1126/science.1208336. URL `http://dx.doi.org/10.1126/science.1208336`.

P. Rowley, J. Thomson, J. Smellie, T. Laudon, K. La Prade, and W. LeMasurier. *C. Alexander Island, Palmer Island, and Ellsworth Land*, pages 256–301. American Geophysical Union (AGU), 1986. ISBN 9781118664728. doi: 10.1029/AR048p0256. URL `https://agupubs.onlinelibrary.wiley.com/doi/abs/10.1029/AR048p0256`.

R. P. Scherer, A. Aldahan, S. Tulaczyk, G. r. Possnert, H. Engelhardt, and B. Kamb. Pleistocene collapse of the West Antarctic Ice Sheet. *Science*, 281(5373):82–85, 1998. doi: 10.1126/science.281.5373.82. URL `http://dx.doi.org/10.1126/science.281.5373.82`.

C. Schoof. Ice sheet grounding line dynamics: Steady states, stability, and hysteresis. *Journal of Geophysical Research*, 112(F03S28), 2007. doi: 10.1029/2006JF000664. URL `http://dx.doi.org/10.1029/2006JF000664`.

D. M. Schroeder. *Characterizing The Subglacial Hydrology Of Thwaites Glacier, West Antarctica Using Airborne Radar Sounding*. PhD thesis, University of Texas at Austin, Autin, Texas, USA, 2014.

D. M. Schroeder, D. D. Blankenship, and D. A. Young. Evidence for a water system transition beneath Thwaites Glacier, West Antarctica. *Proceedings of the National Academy of Sciences*, pages 1–4, 2013. doi: 10.1073/pnas.1302828110. URL `http://www.pnas.org/content/early/2013/07/03/1302828110.abstract`.

D. M. Schroeder, D. D. Blankenship, D. A. Young, and E. Quartini. Evidence for elevated and spatially variable geothermal flux beneath the west antarctic ice sheet. *Proceedings of the National Academy of Sciences*, 111(25):9070–9072, 2014a.

D. M. Schroeder, D. D. Blankenship, D. A. Young, A. E. Witus, and J. B. Anderson. Airborne radar sounding evidence for deformable sediments and outcropping

bedrock beneath Thwaites Glacier, West Antarctica. *Geophysical Research Letters*, 41(20):7200–7208, 2014b. ISSN 1944-8007. doi: 10.1002/2014GL061645. URL http://dx.doi.org/10.1002/2014GL061645.

D. M. Schroeder, D. D. Blankenship, R. K. Raney, and C. Grima. Estimating subglacial water geometry using radar bed echo specularity: application to Thwaites Glacier, West Antarctica. *IEEE Geoscience and Remote Sensing Letters*, 12(3):443–447, 2015. doi: 10.1109/LGRS.2014.2337878. URL http://dx.doi.org/10.1109/LGRS.2014.2337878.

D. M. Schroeder, C. Grima, and D. D. Blankenship. Evidence for variable grounding zone extent and shear margin bed conditions across Thwaites Glacier, West Antarctica. *Geophysics*, 81(1):WA35–WA43, 2016a. doi: 10.1190/geo2015-0122.1. URL http://dx.doi.org/10.1190/geo2015-0122.1.

D. M. Schroeder, H. Seroussi, W. Chu, and D. A. Young. Adaptively constraining radar attenuation and temperature across the Thwaites Glacier catchment using bed echoes. *Journal of Glaciology*, pages 1–8, 2016b. doi: 10.1017/jog.2016.100.

H. Seroussi, E. R. Ivins, D. A. Wiens, and J. Bondzio. Influence of a west antarctic mantle plume on ice sheet basal conditions. *Journal of Geophysical Research: Solid Earth*, 122(9):7127–7155, 2017. doi: 10.1002/2017JB014423. URL https://agupubs.onlinelibrary.wiley.com/doi/abs/10.1002/2017JB014423.

N. M. Shapiro and M. H. Ritzwoller. Inferring surface heat flux distributions guided by a global seismic model: particular application to Antarctica. *Earth and Planetary Science Letters*, 223(1-2):213–224, 2004. doi: 10.1016/j.epsl.2004.04.011. URL http://dx.doi.org/10.1016/j.epsl.2004.04.011.

M. K. Shepard, B. A. Campbell, M. H. Bulmer, T. G. Farr, L. R. Gaddis, and J. J. Plaut. The roughness of natural terrain: A planetary and remote sensing perspective. *Journal of Geophysical Research*, 106(E12):32777–32795, December 2001. doi: 1029/2001JE001429. URL http://dx.doi.org/1029/2001JE001429.

C. S. Siddoway. Tectonics of the West Antarctic Rift System: New light on the history and dynamics of distributed intracontinental extension. In A. K. Cooper, P. J. Barrett, H. Stagg, B. Storey, E. Stump, and W. Wise, editors, *Antarctica: A Keystone in a Changing World*, volume Proceedings of the 10th International Symposium on Antarctic Earth Sciences, pages 91–114, Washington, DC, 2008. The National Acadamies Press.

M. J. Siegert, B. Welch, D. Morse, A. Vieli, D. D. Blankenship, I. Joughin, E. C. King, G. J.-M. C. L. Vieli, A. J. Payne, and R. Jacobel. Ice flow direction change in interior West Antarctica. *Science*, 305(5692):1948–1951, 2004a. doi: 10.1126/science.1101072. URL http://www.sciencemag.org/cgi/content/abstract/305/5692/1948.

M. J. Siegert, B. Welch, D. Morse, A. Vieli, D. D. Blankenship, I. Joughin, E. C. King, G. J.-M. C. L. Vieli, A. J. Payne, and R. Jacobel. Ice flow direction change in interior West Antarctica. *Science*, 305(5692):1948–1951,

2004b. doi: 10.1126/science.1101072. URL `http://www.sciencemag.org/cgi/content/abstract/305/5692/1948`.

R. B. Smith and L. W. Braile. The yellowstone hotspot. *Journal of Volcanology and Geothermal Research*, 61(3-4):121–187, 1994.

B. Storey, I. Dalziel, S. Garrett, A. Grunow, R. t. Pankhurst, and W. Vennum. West antarctica in gondwanaland: crustal blocks, reconstruction and breakup processes. *Tectonophysics*, 155(1-4):381–390, 1988.

B. C. Storey, P. T. Leat, S. D. Weaver, R. J. Pankhurst, J. D. Bradshaw, and S. Kelley. Mantle plumes and Antarctica–New Zealand rifting: evidence from mid-Cretaceous mafic dykes. *Journal of the Geological Society*, 156(4):659–671, 1999.

M. Studinger, R. E. Bell, D. D. Blankenship, C. A. Finn, R. A. Arko, D. L. Morse, and I. Joughin. Subglacial sediments: A regional geological template for ice flow in West Antarctica. *Geophysical Research Letters*, 28(18):3493–3496, September 2001. doi: 10.1029/2000GL011788. URL `http://dx.doi.org/10.1029/2000GL011788`.

S. Tulaczyk, W. B. Kamb, and H. F. Engelhardt. Basal mechanics of Ice Stream B, West Antarctica 2. Undrained plastic bed model. *Journal of Geophysical Research*, 105(B1):483–494, 2000a. doi: 10.1029/1999JB900328. URL `http://dx.doi.org/10.1029/1999JB900328`.

S. Tulaczyk, W. B. Kamb, and H. F. Engelhardt. Basal mechanics of Ice Stream B, West Antarctica 1. Till mechanics. *Journal of Geophysical Research*, 105(B1): 463–482, 2000b. doi: 10.1029/1999JB900329. URL `http://dx.doi.org/10.1029/1999JB900329`.

S. M. Tulaczyk, R. P. Scherer, and C. D. Clark. A ploughing model for the origin of weak tills beneath ice streams: a qualitative treatment. *Quaternary International*, 86(1):59–70, 2001. doi: 10.1016/S1040-6182(01)00050-7. URL `http://www.sciencedirect.com/science/article/B6VGS-44JF5SH-6/2/ec95cd5b67e0f3f355d7271da5c2de8a`.

D. Turcotte and G. Schubert. *Geodynamics*. Cambridge University Press, 2014.

F. M. Van der Wateren and S. A. P. L. Cloetingh. Feedbacks of lithosphere dynamics and environmental change of the cenozoic west antarctic rift system. *Global and Planetary Change*, 23(1-4):1–24, 1999. URL `http://www.sciencedirect.com/science/article/B6VF0-3YJYHD9-1/2/95611dbc2cb3e618d882dcb11e2b8bf4`.

F. M. Van der Wateren, T. J. Dunai, R. T. Van Balen, W. Klas, A. L. L. M. Verbers, S. Passchier, and U. Herpers. Contrasting neogene denudation histories of different structural regions in the transantarctic mountains rift flank constrained by cosmogenic isotope measurements. *Global and Planetary Change*, 23(1-4): 145–172, 1999. URL `http://www.sciencedirect.com/science/article/B6VF0-3YJYHD9-8/2/90ac76bc7af44cc0ee58bad183dd8ffd`.

D. G. Vaughan, H. F. Corr, C. S. Doake, and E. D. Waddington. Distortion of isochronous layers in ice revealed by ground-penetrating radar. *Nature*, 398 (6725):323, 1999.

P. E. Wannamaker, J. A. Stodt, and S. L. Olsen. Dormant state of rifting below the byrd subglacial basin, west antarctica, implied by magnetotelluric (mt) profiling. *Geophysical Research Letters*, 23(21):2983–2986, 1996. doi: 10.1029/96GL02887. URL https://agupubs.onlinelibrary.wiley.com/doi/abs/10.1029/96GL02887.

J. Weertman. Stability of the junction of an ice sheet and ice shelf. *Journal of Glaciology*, 13(67):3–11, 1974.

I. M. Whillans. Radio-echo layers and the recent stability of the west antarctic ice sheet. *Nature*, 264(5582):152, 1976.

P. L. Whitehouse, M. J. Bentley, and A. M. L. Brocq. A deglacial model for Antarctica: geological constraints and glaciological modelling as a basis for a new model of Antarctic glacial isostatic adjustment. *Quaternary Science Reviews*, 32(0):1 – 24, 2012. ISSN 0277-3791. doi: http://dx.doi.org/10.1016/j.quascirev.2011.11.016. URL http://www.sciencedirect.com/science/article/pii/S0277379111003726.

D. S. Wilson and B. P. Luyendyk. Bedrock platforms within the Ross Embayment, West Antarctica: hypotheses for ice sheet history, wave erosion, Cenozoic extension, and thermal subsidence. *Geochemistry, Geophysics, Geosystems*, 7

(12), 2006. doi: 10.1029/2006GC00129. URL `http://dx.doi.org/10.1029/2006GC00129`.

F. Wobbe, K. Gohl, A. Chambord, and R. Sutherland. Structure and breakup history of the rifted margin of west antarctica in relation to cretaceous separation from zealandia and bellingshausen plate motion. *Geochemistry, Geophysics, Geosystems*, 13(4), 2012.

E. Wolfenden, C. Ebinger, G. Yirgu, P. R. Renne, and S. P. Kelley. Evolution of a volcanic rifted margin: Southern red sea, ethiopia. *Geological Society of America Bulletin*, 117(7-8):846–864, 2005.

G. Wörner. Lithospheric dynamics and mantle sources of alkaline magmatism of the Cenozoic West Antarctic Rift System. *Global and Planetary Change*, 23(1): 61–77, 1999. doi: https://doi.org/10.1016/S0921-8181(99)00051-X. URL `http://www.sciencedirect.com/science/article/pii/S092181819900051X`.

D. A. Young, S. D. Kempf, D. D. Blankenship, J. W. Holt, and D. L. Morse. New airborne laser altimetry over the Thwaites Glacier Catchment, West Antarctica. *Geochemistry, Geophysics, Geosystems*, 9(6):Q06006, 2008. doi: 10.1029/2007GC001935. URL `http://dx.doi.org/10.1029/2007GC001935`.

D. A. Young, D. M. Schroeder, D. D. Blankenship, S. D. Kempf, and E. Quartini. The distribution of basal water between Antarctic subglacial lakes from radar sounding. *Philosophical Transactions of the Royal Society A*, 374(20140297):1–21, 2015. doi: 10.1098/rsta.2014.0297. URL `http://dx.doi/org/10.1098/rsta.2014.0297`.